scientific reports

Check for updates

OPEN

Identification of prognostic and therapeutic biomarkers associated with macrophage and lipid metabolism in pancreatic cancer

Lili Wu[1,5], Feihong Liang[2,3,5], Changgan Chen[2,5], Yaxin Zhang[2], Heguang Huang[2] & Yu Pan[2,4]✉

Although macrophages and lipid metabolism significantly influence the progression of various cancers, their precise roles in pancreatic cancer (PC) remain unclear. This study focuses on identifying and validating biomarkers associated with macrophage-related genes (MRGs) and lipid metabolism-related genes (LMRGs), providing new targets and strategies for therapeutic intervention. This research utilized datasets from TCGA-PAAD, GSE62452, and GSE57495. Candidate genes were identified by overlapping differentially expressed genes with MRGs from WGCNA and LMRGs. Regression analyses were performed to pinpoint potential biomarkers and construct a risk model, which underwent evaluation. A nomogram was subsequently developed and validated. Additional analyses, including functional enrichment, somatic mutation profiling, immune landscape assessment, and RT-qPCR, were performed to investigate the underlying biological mechanisms in PC. The study identified ADH1A, ACACB, CD36, CERS4, PDE3B, ALOX5, and CRAT as biomarkers for PC. RT-qPCR results revealed reduced expression of ADH1A, ACACB, CD36, CERS4, PDE3B, and CRAT in tumor samples compared to adjacent tissues, whereas ALOX5 expression was significantly elevated in tumor samples. A risk model utilizing these biomarkers classified PC patients into high- and low-risk cohorts, with high-risk patients showing lower survival probabilities. Subsequently, risk score and N stage were identified as independent prognostic factors, leading to the development of a nomogram. Notably, both risk cohorts showed significant enrichment in the "cell cycle" pathway. Furthermore, TP53 mutations were prevalent in both high-risk (76%) and low-risk (50%) cohorts. Correlation analysis indicated that PVRL2 (an immunosuppressive factor), CD276 (an immunoactivator), and CCL20 (a chemotactic factor) had the highest positive correlation with the risk score. In this study, ADH1A, ACACB, CD36, CERS4, PDE3B, ALOX5, and CRAT were identified as biomarkers for PC, with their expression levels validated in clinical samples. These findings offered a potential theoretical foundation for developing targeted treatments for PC.

Keywords Pancreatic cancer, Macrophage, Lipid metabolism, Biomarkers

Abbreviations

PC	Pancreatic cancer
MRGs	Macrophage-related genes
LMRGs	Lipid metabolism-related genes
DEGs	Differentially expressed genes
TCGA-PAAD	The cancer genome atlas-pancreatic adenocarcinoma
WGCNA	Weighted correlation network analysis
RT-qPCR	Reverse transcription-quantitative PCR
KRAS	Kirsten rat sarcoma viral oncogene homolog
SLC25A1	Solute carrier family 25 member 1

[1]Department of Surgical Nursing, Fujian Medical University Union Hospital, Fuzhou, People's Republic of China. [2]Department of General Surgery, Fujian Medical University Union Hospital, No. 29 Xinquan Road, Fuzhou 350001, People's Republic of China. [3]The Cancer Center, Fujian Medical University Union Hospital, Fuzhou, People's Republic of China. [4]Central Laboratory, Fujian Medical University Union Hospital, Fuzhou, People's Republic of China. [5]Lili Wu, Feihong Liang and Changgan Chen contributed equally to this work. ✉email: yupan199002@163.com

CPT1A	Carnitine palmitoyltransferase 1A
CPT1B	Carnitine palmitoyltransferase 1B
FASN	Fatty acid synthase
PDAC	Pancreatic ductal adenocarcinoma
ACLY	Acetyl-CoA carboxylase
LDLR	Low-density lipoprotein receptor
TME	Tumor microenvironment
TAMs	Tumor-associated macrophages
Tregs	Regulatory T cells
Bregs	Regulatory B cells
MDSCs	Myeloid-derived suppressor cells
CAFs	Cancer-associated fibroblasts
oxLDL	Oxidized low-density lipoprotein
PGE2	Prostaglandin E2
TCGA	The Cancer Genome Atlas
GEO	Gene expression omnibus
GO	Gene ontology
KEGG	Kyoto encyclopedia of genes and genomes
PPI	Protein–protein interaction
HR	Hazard ratio
PH	Proportional hazards
LASSO	Least absolute shrinkage and selection operator
K–M	Kaplan–Meier
AUC	Area under the curve
OS	Overall survival
DCA	Decision curve analysis
MSigDB	Molecular signatures database
GSEA	Gene set enrichment analysis
NES	Normalized enrichment score
TMB	Tumor mutational burden
H-TMB	High-TMB
L-TMB	Low-TMB
IC50	Half maximal inhibitory concentration
MDSC	Myeloid-derived suppressor cells
Cor	Correlation coefficient
BP	Lipid catabolic process
CC	Peroxisomal matrix
MF	Lipase activity
Cox	Cox proportional hazards model
ADH1A	Alcohol dehydrogenase 1A
ACACB	Acetyl-CoA carboxylase beta
CD36	CD36 molecule
CERS4	Ceramide synthase 4
PDE3B	Phosphodiesterase 3B
ALOX5	Arachidonate 5-lipoxygenase
CRAT	Carnitine O-acetyltransferase
TP53	Tumor protein P53
CDKN2A	Cyclin dependent kinase inhibitor 2A
SMAD4	SMAD family member 4
PVRL2	Nectin cell adhesion molecule 2
PYGL	Glycogen phosphorylase L
CCND2	Cyclin D2
BCAT1	Branched chain amino acid transaminase 1
KRT7	Keratin 7
MMP9	Matrix metalloproteinase 9
cGMP	Cyclic guanosine monophosphate
cAMP	Cyclic adenosine monophosphate
CD160	CD160 molecule
CD276	CD276 molecule
CCL20	C–C motif chemokine ligand 20
CCR6	C–C motif chemokine receptor 6
CCL14	C–C motif chemokine ligand 14

Pancreatic cancer (PC) is experiencing a rising incidence and is considered one of the deadliest human malignancies[1], with a current 5-year overall survival rate of less than 9%[2]. Patients are often diagnosed at advanced stages and a lack of effective early cancer screening methods. While surgical resection remains the only potential cure, treatment options are severely limited for advanced diseases, including those with distant metastasis or locally advanced tumors[2]. Consequently, early detection of invasive precursors and the identification of molecular therapeutic targets are critical for improving survival outcomes. Furthermore, routine screening

for PC is not recommended for the general population, since even extremely sensitive screening tests can lead to unacceptable false-positive results, but emerging evidence indicates that monitoring specific high-risk groups by using biomarkers may enhance prognosis[3]. This underscores the urgent need to explore new biomarkers that hold clinical significance for screening at-risk PC patients.

Lipids, which include fats, phospholipids and sterols, are vital nutrients that serve as structural components of cells, organelles, and nuclear membranes[4]. Moreover, they are crucial for energy storage and act as second messengers in intracellular signaling, especially during nutrient deprivation[2]. Increasingly, research indicates that lipids and their metabolites play key roles in complex signaling pathways. Aberrant lipid metabolism is strongly implicated in the initiation and progression of PC[5], influencing processes such as membrane biosynthesis, lipid turnover, and lipid-mediated signaling. During tumor progression, cancer cells exploit lipid metabolism to support rapid proliferation, survival, migration, invasion, and metastasis[6–8]. Studies have reported that in $KRAS^{G12D}$-specific mouse models of pancreatic acinar cells, upregulation of SLC25A1 enhances the level of Carnitine Palmitoyltransferase 1A (CPT1A) and 1B (CPT1B), and Fatty Acid Synthase (FASN), accelerating pancreatic tumorigenesis[9]. The oncogenic KRAS is a primary driver of PC development, regulating the storage and utilization of lipid droplets, with the expression of lipid droplet-associated genes correlating with overall survival in PC patients[9]. In various tumors, including PC, reduced expression of Acetyl-CoA Carboxylase (ACLY) leads to decrease tumor cell proliferation and inhibit tumor progression[10,11]. Additionally, downregulation of Low-Density Lipoprotein Receptor reduces cholesterol uptake and tumor proliferation in PC, small cell lung cancer, and breast cancer cells[12–14].

PC is characterized by a complex tumor microenvironment (TME), comprising a dense stromal matrix interspersed with a limited number of tumor cells and a diverse array of immunosuppressive components[15,16]. Among these, tumor-associated macrophages (TAMs) serve as critical regulators within the TME, playing a central role in modulating the tumor's immune landscape[17,18]. Macrophages, a type of innate immune cell first described by Élie Metchnikoff in the nineteenth century, play a crucial role in engulfing foreign substances[19,20]. They are primarily classified into two subtypes: classically activated (M1) and alternatively activated (M2). M1 macrophages are inflammatory and generally considered anti-tumor, while M2 macrophages are associated with anti-inflammatory responses and are primarily linked to tumor progression[21,22]. Recent research has shown that lipids and their metabolites significantly influence macrophage responses to pathogens, phagocytosis, ferroptosis, and inflammatory processes[23]. Among the various lipids, oxidized low-density lipoprotein (oxLDL) has been extensively studied for its role in inducing M2 macrophage polarization[24,25]. Similarly, Similarly, arachidonic acid-derived metabolites, including prostaglandin E2 (PGE2), are known to enhance the M2 phenotype[26]. This M2 polarization is further facilitated by increased lipid accumulation observed in TAMs across various cancers in both humans and mice[27]. Thus, the relationship between lipid metabolism and macrophage is pivotal in understanding the tumor-promoting environment in cancer. However, there is a lack of in-depth studies on the relationship between macrophage-related genes (MRGs) and lipid metabolism-related genes (LMRGs) with PC.

This study employed a range of bioinformatics methods to identify biomarkers associated with macrophage and lipid metabolism in PC. Then these biomarkers in clinical samples were validated through RT-qPCR. In addition, Conducted functional explorations that included constructing risk and prognostic models, performing functional enrichment analysis, analyzing somatic mutations, assessing the immune landscape, and predicting drug responses were performed to investigate the differences between high-risk and low-risk PC patients. These analyses provide new insights into the treatment and prognosis of PC.

Materials and methods

Data collection

TCGA-PAAD dataset, which included transcriptomic data, clinical and survival information for PC patients, was sourced from the TCGA database. This dataset consisted of 178 tumor pancreatic tissue samples (with survival information available for 177 of these samples), and 4 normal pancreatic tissue samples. Additionally, this study incorporated data from the GSE62452 and GSE57495 datasets, retrieved from the GEO database. Specifically, the GSE62452 dataset comprised 69 tumor and 61 normal pancreatic tissue samples, based on the GPL6244 platform Meanwhile, GSE57495 (GPL15048 platform) comprised 63 tumor pancreatic tissue samples. Furthermore, a total of 1,045 lipid metabolism-related genes (LMRGs) were identified from the literature (Supplementary Table 1)[28].

Immune infiltration analysis

Immune infiltration analysis in tumor and adjacent normal samples was analyzed using the GSE62452 dataset. The ssGSEA algorithm from "immunedeconv" package (v 2.1.0) was employed to calculate the infiltration scores for 28 immune cell types[29,30]. Next, the Wilcoxon test was applied to compare the infiltration scores of these immune cells between tumor and normal samples, identifying differential immune cells ($P<0.05$) for further investigation. Subsequently, Spearman correlation analysis was performed using the 'cor' function to explore the relationships among the differential immune cells, considering correlations significant at $|cor|>0.3$ and $P<0.05$.

WGCNA

In the GSE62452 dataset, we used the "WGCNA" package (v 1.72-5) for WGCNA to identify macrophage—related key modules[31]. First, we excluded outlier samples through hierarchical clustering. Then, we determined the optimal soft threshold that made the scale-free fitting index R^2 greater than 0.9 and the mean connectivity approach zero. A co-expression matrix was constructed with a minimum module gene number (minModuleSize) of 50 and a module merging height threshold (mergeCutHeight) of 0.4, and each module was distinguished by color. We used Pearson correlation analysis ($|cor|>0.3$, $P<0.05$) to screen out the key modules most strongly correlated with the macrophage trait and the macrophage-related genes (MRGs) within them.

To ensure the reliability of the WGCNA analysis, we calculated the scale-free fitting index and mean connectivity under different soft thresholds to select the optimal soft threshold, ensuring that the node connectivity in the network conformed to the power-law distribution, which is a key assumption in WGCNA analysis. We also evaluated the network topological structures under different soft threshold values by plotting the scale-free fitting index diagrams.

Differential expression analysis

Differentially expressed genes (DEGs) between tumor and normal samples in the GSE62452 dataset were identified using the "limma" package (v 3.54.0)[31], with thresholds set at $|\log_2 FC| > 0.5$ and $P < 0.05$. Visualization of the DEGs was performed using a volcano plot and a heatmap. The volcano plot was generated with the "ggplot2" package (v 3.4.1)[32], and a heatmap created using the "ComplexHeatmap" package (v2.14.0), showcasing the top 10 upregulated and downregulated genes ranked by $|\log_2 FC|$.[33].

Function analysis

Candidate genes were obtained by intersecting DEGs, MRGs, and LMRGs using the "ggvenn" package (v0.1.9)[34]. Functional enrichment analysis was conducted using the "clusterProfiler" package (v4.7.1.3) to perform GO and KEGG pathway analysis, with a significance threshold of $P < 0.05$[35–37]. To explore protein–protein interactions, a PPI network was constructed via the STRING database (confidence score > 0.4). Outlier genes were filtered, and the network was visualized using Cytoscape (v3.9.1)[38].

Determination of the biomarkers

Based on the candidate genes, survival-related genes were identified by univariate Cox regression analysis [hazard ratio (HR) ≠ 1, $P < 0.05$] and proportional hazards (PH) assumption test ($P > 0.05$). Notably, univariate Cox regression analysis was conducted by "survival" package (v 3.5.3)[39]. Subsequently, the least absolute shrinkage and selection operator (LASSO) was applied to refine biomarker selection, employing the "glmnet" package (v4.1.4)[40]. When choosing the lambda value in the LASSO regression, we gave priority to the prediction performance of the model and the robustness of the biomarkers. Since lambda.min corresponded to the model with the minimum cross—validation error, it could provide the best prediction performance and contain more potential biomarkers. While lambda.1se offered a more concise model, it might sacrifice prediction accuracy. Moreover, the objectives and resources of our study allowed for the subsequent validation of more variables. Therefore, we chose lambda.min as the optimal model. The optimal lambda value was determined through tenfold cross-validation.

To verify the proportionality assumption of the Cox regression models, we used the cox.zph function from the "survival" package to calculate the Schoenfeld residuals. This function was used to calculate the Schoenfeld residuals and test the time—dependent covariates. For each univariate Cox model, we extracted the chi–square statistic (chisq), degrees of freedom (df), and *p*-value. Covariates with a *p*-value greater than 0.05 were considered to satisfy the PH assumption, indicating that their hazard ratios remained constant over time. Covariates that did not meet the PH assumption ($p < 0.05$) were excluded from further analysis to ensure the validity of the Cox regression models.

Establishment and validation the risk model

A risk model was built based on the identified biomarkers, with the risk score calculated as follows:

$$riskscore = \sum_{i=1}^{n} (coefi * Xi)$$

where "coef" represents the coefficients of the biomarkers in LASSO analysis and "expression" indicates their expression levels.

Afterward, to evaluate the risk model, Using survival data from 177 PC patients in the TCGA-PAAD dataset, patients were stratified into high- and low-risk cohorts based on an optimal risk score cutoff. KM survival curves were plotted to compare survival probabilities between the two cohorts ($P < 0.05$). ROC curves for 1-, 2-, and 3-year survival predictions were constructed using the "survivalROC" package (v1.0.3.1)[41], with all AUC values exceeding 0.6. Additionally, a heatmap was generated to visualize biomarker expression patterns across the cohorts.

Besides, to validate the risk model, the same methods were applied to the GSE57495 dataset, which included 63 samples with complete survival information.

Clinical characteristics analysis

To thoroughly analyze the distribution of clinical characteristics in the high- and low-risk cohorts from the TCGA-PAAD dataset, a heatmap was created. Additionally, the proportions of clinical characteristic subgroups in two risk cohorts were explored, including age (> 60 and ≤ 60), stage (I–IV), N stage (N0–N1), gender (female and male), T stage (T1–T4), and G stage (G1–G4).

Development and assessment of a nomogram

In PC patients with complete survival information from the TCGA-PAAD dataset, the risk score was integrated with clinical characteristics. Then, univariate Cox analysis (HR ≠ 1 and $P < 0.05$), PH assumption tests ($P > 0.05$), and multivariate Cox regression analysis (HR ≠ 1 and $P < 0.05$) were performed to identify independent prognostic factors for PC patients. Specifically, we first included all potential clinical variables such as T stage, N stage,

tumor grade, age, gender, and risk score in the univariate Cox regression analysis. The univariate Cox regression analysis was performed using the "survival" package (v 3.5.3) in R. After excluding these non—significant variables, we conducted the proportional hazards (PH) assumption test and multivariate Cox regression analysis on the remaining variables. Finally, the independent prognostic factors were determined. Based on independent prognostic factors, a nomogram was developed with the "rms" package (v6.5.0) to predict overall survival (OS) at 1, 2, and 3 years[42]. To assess model accuracy and ROC curves for 1-, 2-, and 3-year survival were generated using the "survivalROC" package (AUC > 0.6). Next, We used the C-index (concordance index) to evaluate the accuracy of the model. First, we used the cph function in the "rms" package (v 7.0.0)[43] to fit the Cox proportional hazards model, establishing the relationship between the predictive factors and survival outcomes. Then, we calibrated the fitted Cox model through the calibrate function. Additionally, Decision Curve Analysis (DCA) was performed to evaluate the nomogram's predictive ability.

Overall, these analyses provided a comprehensive evaluation of the nomogram's accuracy and clinical utility in predicting the mortality rate of PC based on the identified independent prognostic factors.

Function analysis of high- and low-risk cohorts

To explore the biological pathways distinguishing high- and low-risk cohorts in TCGA-PAAD, functional enrichment analysis was performed. Differential gene expression analysis between the two risk groups was conducted using "DESeq2" (v1.42.0)[44], with DEGs ranked by $\log_2$ fold change ($\log_2$FC). Gene set enrichment analysis (GSEA) was conducted using the "clusterProfiler" package, with the "c2.cp.kegg.v2022.1.Hs.symbols.gmt" gene set from MSigDB. Pathways were considered significant if |NES| > 1 and $P < 0.05$.

Somatic mutation analysis

Somatic mutation data for PC patients from TCGA-PAAD were analyzed using the "maftools" package (v2.18.0)[45]. The top 20 most frequently mutated genes were identified for both high- and low-risk cohorts, and waterfall plots were generated to visualize these mutations. Tumor mutational burden (TMB) scores were calculated and compared between risk groups using the "maftools" and "rstatix" packages, with statistical significance assessed by the Wilcoxon test ($P < 0.05$)[46].

Spearman's correlation analysis was also performed to explore the relationship between TMB and risk scores. Survival analysis using Kaplan–Meier curves was conducted to compare survival across various combinations of TMB and risk groups (H-TMB + high-risk, H-TMB + low-risk, L-TMB + high-risk, and L-TMB + low-risk).

Immune landscape analysis

In this study, to effectively guide PC immunotherapy, we utilized 20 immunosuppressive factors, 38 immunoactivator factors, and 36 chemotactic factors sourced from the literature[47]. Specifically, the expression of these factors in high- and low-risk cohorts, as well as in different clinical characteristic subgroups, was analyzed and presented in heatmap. Additionally, Spearman correlation analyses were conducted to explore the relationships between immunosuppressive factors and risk scores, immunoactivator factors and risk scores, and chemotactic factors and risk scores (|cor| > 0.3 and $P < 0.05$).

Drug sensitivity analysis

Generally, a higher IC_{50} indicates lower drug sensitivity. To assess the drug sensitivity of PC patients in high- and low-risk cohorts from the TCGA-PAAD dataset, IC_{50} values for 138 conventional drugs were calculated using the "pRRophetic" package (v 0.5)[48]. Subsequently, the Wilcoxon test was utilized to compare the differences in IC_{50} between the two risk cohorts ($P < 0.05$). The top 10 drugs with the most significant differences, ranked by P value (from low to high), were displayed. Additionally, he three-dimensional structures of these drugs were visualized using PubChem (https://pubchem.ncbi.nlm.nih.gov).

Evaluation biomarkers expression levels

In GSE62452 datasets, Wilcoxon tests were utilized to compare the expression difference between tumor and adjacent normal samples ($P < 0.05$).

Besides, to validate the expression of biomarkers in clinical samples, reverse transcription quantitative PCR (RT-qPCR) analysis was performed as priviously described[49]. The primer sequences are listed in Supplementary Table 2. Specifically, a total of 20 samples (10 tumor-adjacent and 10 tumor tissues) were acquired from the clinic in the Fujian Medical University Union Hospital. All participants were given informed consent.

This study had the approval of the Ethics Review Committee, Fujian Medical University Union Hospital (approval number: 2023KJCXC028). All research was performed in accordance with relevant guidelines and regulations and in accordance with the Declaration of Helsinki.

Statistical analysis

The R (v 4.2.2) was utilized to conduct statistical analysis. Differences analysis between groups was executed via the Wilcoxon test ($P < 0.05$).

Results

Identification of 2,860 MRGs

The overall workflow of this work is presented in Fig. 1. The immune infiltration proportions of 28 immune cell types in tumor and normal samples from the GSE62452 dataset were illustrated in Supplementary Fig. 1A. Notably, 18 immune cell types displayed differential infiltration between the tumor and normal samples ($P < 0.05$). Specifically, macrophages, activated CD4 T cells, and activated dendritic cells were notably more abundant in tumor samples, while eosinophils were found to be more abundant in the normal samples (Supplementary

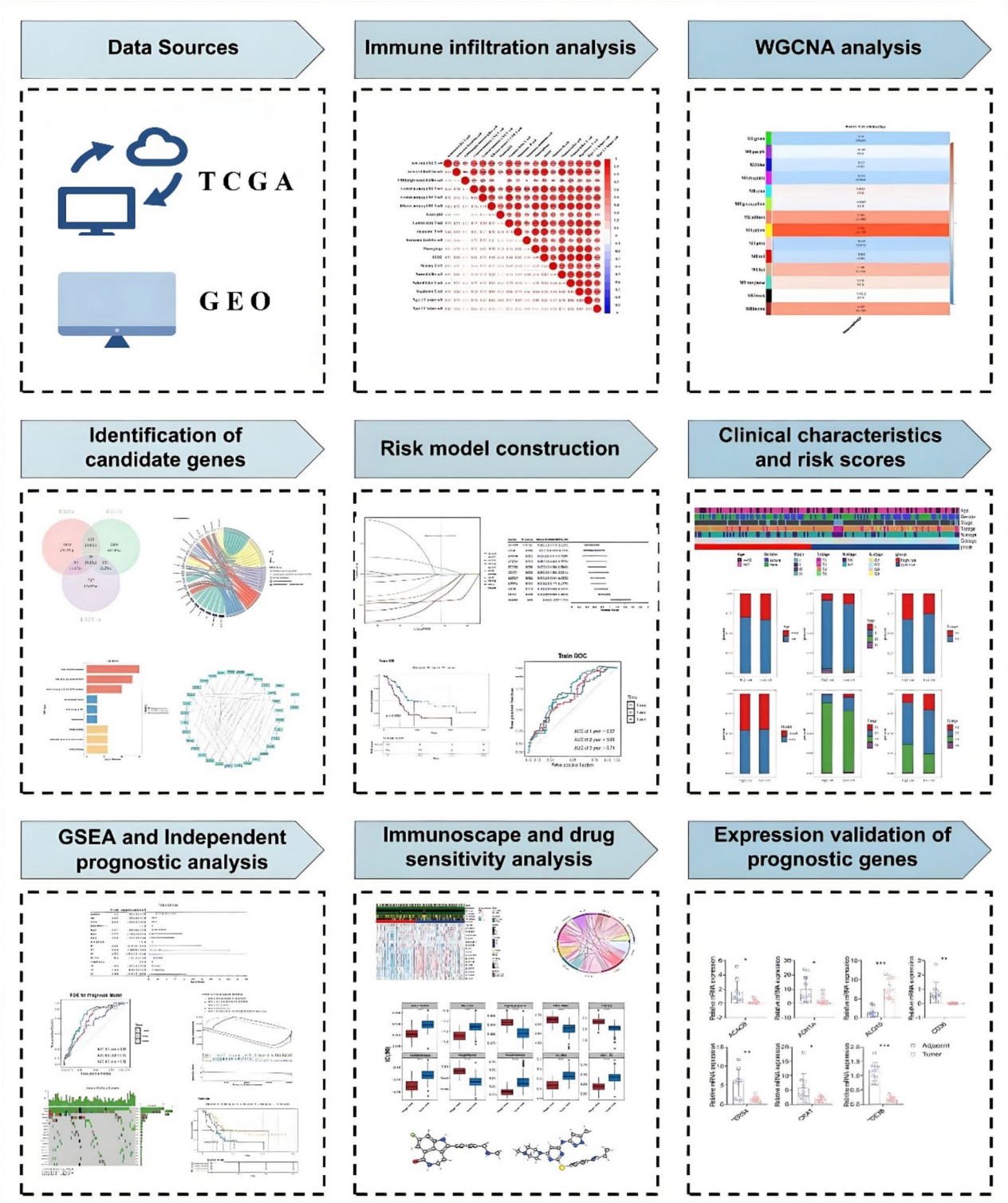

Fig. 1B). Further analysis indicated that regulatory T cells had the strongest positive correlation with myeloid-derived suppressor cells (MDSC) (cor = 0.91, $P < 0.05$), and macrophages were positively correlated with effector memory CD8 T cells and immature B cells (cor = 0.82, $P < 0.05$) (Supplementary Fig. 1C). In the WGCNA analysis of the GSE62452 dataset, no outlier samples were detected or removed (Supplementary Fig. 2A). The optimal power value was determined to be 12, as it exceeded the red line indicating an R^2 value of 0.9, with mean connectivity approaching 0 (Supplementary Fig. 2B). Modules were merged from the co-expression matrix, resulting in the identification of 14 gene modules (excluding a gray module for unclassified genes), each represented by a distinct color (Supplementary Fig. 2C). The MEyellow module exhibited the highest positive correlation with macrophages (cor = 0.793, $P = 5 \times 10^{-16}$), whereas the MEgreen module demonstrated a significant negative correlation with macrophages (cor = −0.361, $P = 0.002$) (Supplementary Fig. 2D).

◀**Fig. 1**. A workflow of the study. Data acquisition: Pancreatic cancer—related datasets such as TCGA–PAAD, GSE62452, and GSE57495 were obtained from The Cancer Genome Atlas (TCGA) and the Gene Expression Omnibus (GEO), laying the foundation for subsequent analyses. Immune infiltration analysis: Analyze the data to explore the infiltration of immune cells in pancreatic cancer and clarify the role of the immune system. WGCNA analysis: Construct a gene co-expression network, identify key gene modules, and explore gene relationships. Identification of candidate genes: Overlap and analyze differentially expressed genes with macrophage—related genes (MRGs) and lipid metabolism—related genes (LMRGs) obtained from WGCNA analysis to determine relevant candidate genes. Risk model construction: Based on candidate genes, construct and evaluate a risk model through regression analysis and other methods to classify patients into different risk levels. Clinical characteristics and risk scores: Calculate risk scores by combining clinical characteristics, analyze the relationships between risk scores and clinical indicators to assist in clinical diagnosis and treatment. Gene set enrichment and prognostic analysis: Use Gene Set Enrichment Analysis (GSEA) to explore the pathways of candidate genes, and conduct independent prognostic analysis to evaluate their impact on prognosis. Immune landscape and drug sensitivity analysis: Analyze the immune landscape, study the relationships between immune—related genes and risk scores, and screen out drugs sensitive to different risk groups. Validation of prognostic genes: Use techniques such as RT—qPCR to validate the expression levels of candidate (prognostic) genes in clinical samples and confirm their reliability as biomarkers.

Consequently, the 1,485 genes within the MEyellow module and 1,375 genes within the MEgreen module were identified as MRGs, totaling 2,860 genes.

Discovery and functional exploration of candidate genes

Differential expression analysis identified 1,553 DEGs (tumor vs. normal), including 1,080 upregulated and 473 downregulated genes in tumor samples (Fig. 2A,B). By intersecting the 1,553 DEGs with 2,860 MRGs, and 1,045 LMRGs, the 38 candidate genes were identified (Fig. 2C). Functional enrichment analysis revealed that these 38 candidate genes were significantly associated with 513 GO terms, which included 416 BPs, 84 MFs, and 13 CCs, as well as 34 KEGG pathways. Notable GO terms included "lipid catabolic process" (BP), "peroxisomal matrix" (CC), and "lipase activity" (MF) (Fig. 2D). In the KEGG pathways, the candidate genes were significantly enriched in "fat digestion and absorption", "metabolism of xenobiotics by cytochrome P450", and "retinol metabolism", among others (Fig. 2E). Furthermore, after removing four outlier genes, a PPI network was constructed, comprising 34 nodes and 97 edges (Fig. 2F). Notably, ACACB was found to interact closely with CD36 and SCD5 within this network. In summary, these findings highlighted candidate genes and their functional associations, paving the way for further investigation into their roles in tumor biology.

Construction of well-performing risk model

From an initial set of 38 candidate genes, 11 survival-related genes were identified using univariate Cox regression analysis ($HR \neq 1$, $P < 0.05$) and the PH assumption test ($P > 0.05$) (Fig. 3A, Supplementary Table 3). The LASSO method further refined this to seven biomarkers: ADH1A, ACACB, CD36, CERS4, PDE3B, ALOX5, and CRAT, based on a lambda min of 0.043 with non-zero regression coefficients (Fig. 3B).

A risk model was then developed using these seven biomarkers identified from LASSO analysis, risk score was calculated based on the coefficients of the biomarkers in LASSO analysis (Supplementary Table 4) and expressions of biomarkers. This risk model enabled for the stratification of 177 PC patients with complete survival data from the TCGA-PAAD dataset into 76 high-risk and 101 low-risk cohorts at an optimal cutoff risk score of − 1.689375. Similarly, 63 PC patients from the GSE57495 dataset were classified into 26 high-risk and 37 low-risk cohorts using an optimal cutoff risk score of − 6.941261. Subsequent analyses, including risk curves and survival status distribution diagrams, showcased a clear distinction between high-risk and low-risk cohorts in the TCGA-PAAD dataset, with high-risk patients demonstrating higher mortality rates and shorter survival times (Fig. 3C). K–M curves indicated significantly lower survival probabilities for high-risk patients in the TCGA-PAAD dataset ($P < 0.05$) (Fig. 3D). ROC curves revealed AUC values exceeding 0.6, underscoring the robust predictive performance of the risk model (Fig. 3E). Additionally, a heatmap illustrated that the seven biomarkers were expressed at lower levels in the high-risk cohort from the TCGA-PAAD dataset (Fig. 3F). Importantly, these results were consistently validated in the GSE57495 dataset (Supplementary Fig. 3A–D). Overall, these findings emphasized the utility of the developed risk model in stratifying PC patients, potentially facilitating more personalized treatment strategies and improved disease management.

Association of clinical characteristics with risk score

A heatmap illustrated the relationship between clinical characteristics and risk scores, revealing that G3 and G4 stages were more frequent in the high-risk cohort compared to the low-risk cohort (Fig. 4A). In contrast, the distributions of age and gender among the subgroups were relatively similar across both cohorts. Additionally, A higher proportion of high-risk patients were classified in advanced tumor stages (G3 and G4), whereas low-risk patients were more commonly in T1 and T2 stages (Fig. 4B). In summary, these findings suggested that tumor grade might be a critical factor in risk stratification for PC patients, emphasizing the need for tailored management strategies based on individual clinical characteristics.

Establishment good nomogram based on independent prognostic factors

Univariate Cox regression analysis demonstrated that when evaluating the associations between multiple variables and the prognosis of PC, the risk score ($P < 0.05$, HR = 3.989, 95% CI 2.067–7.696) and N stage ($P < 0.05$,

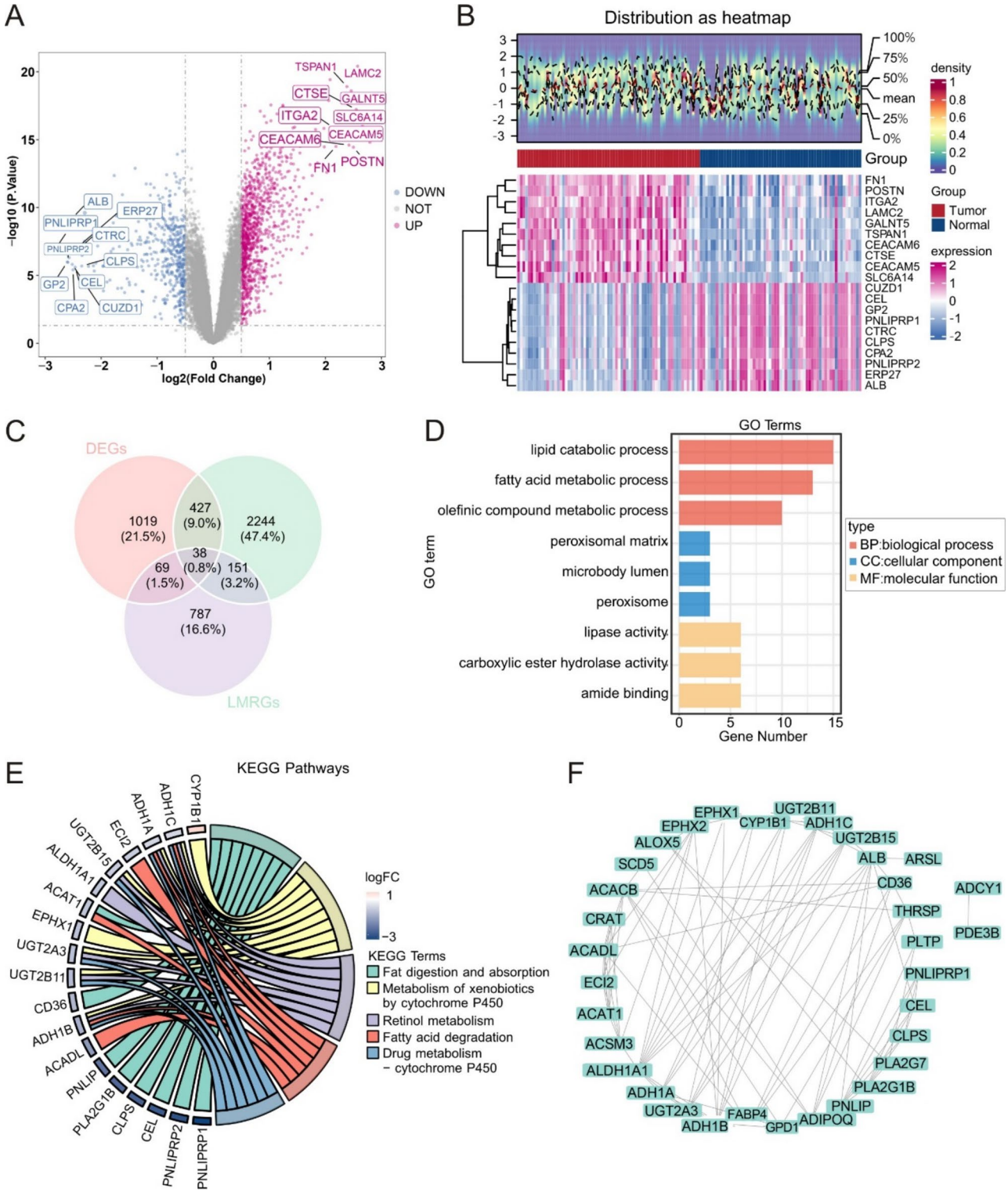

Fig. 2. Screening for candidate genes. (**A**) Differential gene volcano plot, purple dots represent upregulated genes, blue dots represent downregulated genes, and gray dots indicate non-significant genes. (**B**) Differential gene heat map. The top half is a heatmap of the expression density of the 10 genes with the largest multiplicity of sample differences; the bottom half is an expression heatmap. (**C**) Venn diagram of candidate genes in PC. (**D**) GO enrichment analysis histogram of candidate gene. (**E**) KEGG enrichment analysis: the left side lists the gene names, and the right side highlights enriched functional pathways. (**F**) Interaction network diagram of candidate genes. Each square represents a protein and the connecting lines represent having an interaction relationship.

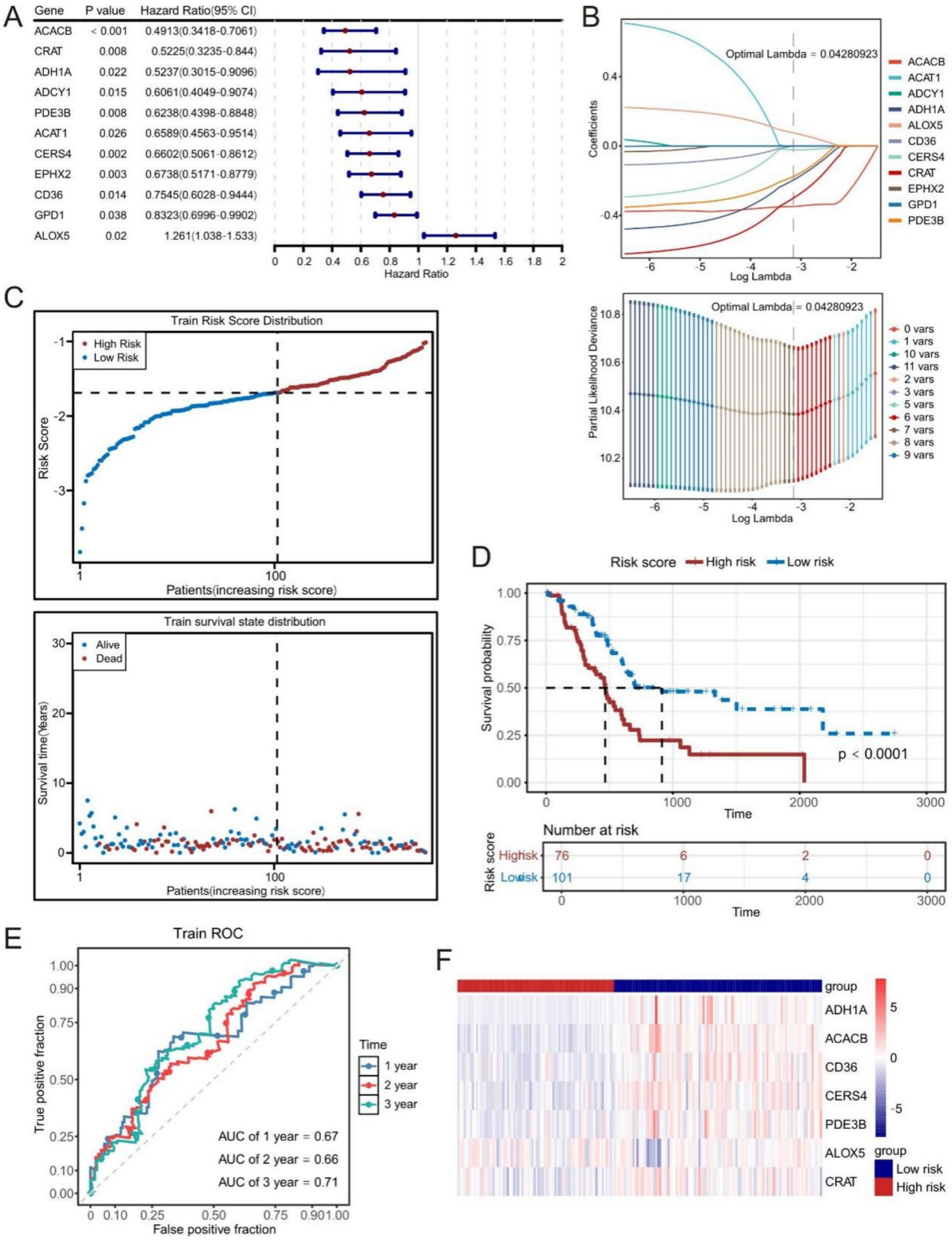

Fig. 3. Screening for prognostic genes and risk model construction. (**A**) Univariate cox forest plot of prognosis-related genes. (**B**) Lasso regression analysis. The left panel showed the path of Lasso regression coefficients; the right panel showed the Lasso cross-validation curve. (**C**) Risk curves and survival state distributions for the training set TCGA-PAAD sample. (**D**) K–M plot for low and high risk groups in training set TCGA-PAAD. (**E**) ROC curve for assessing the predictive performance of the risk model in the TCGA-PAAD training set. (**F**) Heatmap illustrating the expression levels of prognostic genes across low and highrisk groups in the validation set. The color scale represented the gene expression levels, where red indicated high expression and blue indicated low expression. The normalization method employed was z-score normalization. Each gene's expression values across all samples were standardized, resulting in a mean of 0 and a standard deviation of 1 after standardization.

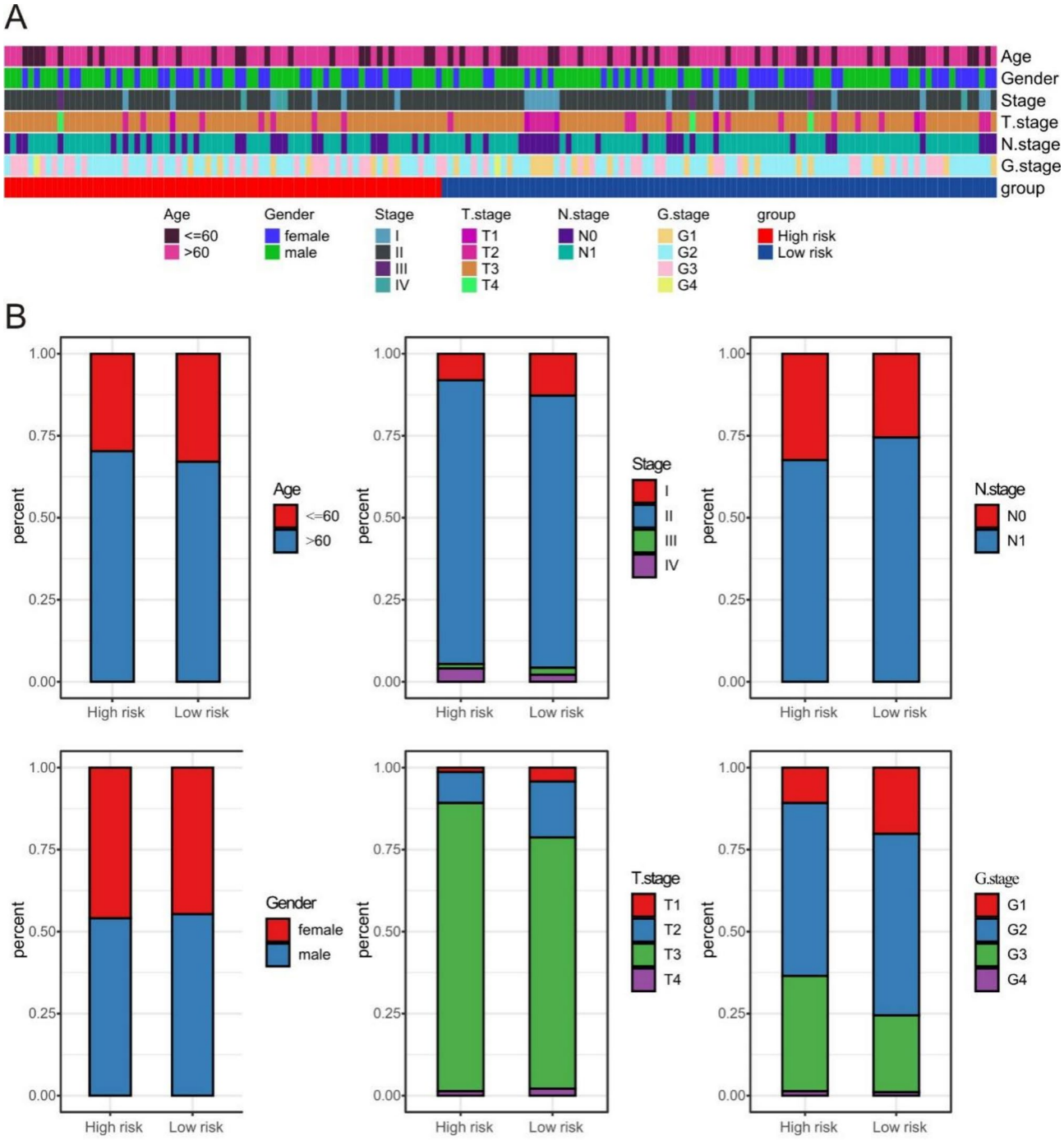

Fig. 4. Analysis of the correlation between clinical characteristics and risk scores. (**A**) Heatmap of clinical characteristics and risk scores. Horizontal coordinates are different samples, vertical coordinates are subgroups and different clinical characteristics. (**B**) Distribution of risk scores for different clinicopathologic features. The horizontal axis indicated the low- and high-risk groups, and the vertical axis indicates the percentage within each group.

HR = 2.231, 95% CI 1.313–3.379) were significantly associated with the prognosis, while some variables such as gender ($P = 0.221$) showed no significant association. Meanwhile, the 2—year AUC values of each factor were presented to assist in assessing the predictive efficacy (Fig. 5A). For the proportional—hazards assumption test, the *P*-value of the Global Schoenfeld test was 0.7521, and the *P*-values of the individual Schoenfeld tests for most indicators were greater than 0.05, indicating that the proportional—hazards assumption was valid and the Cox regression model was applicable (Fig. 5B). In the multivariate Cox regression analysis, after adjusting for other factors, the risk score ($P < 0.05$, HR = 4.32, 95% CI 2.164–8.622) and N stage ($P < 0.05$, HR = 2.18, 95% CI 1.282–3.707) were identified as independent prognostic factors, which had a significant impact on the survival

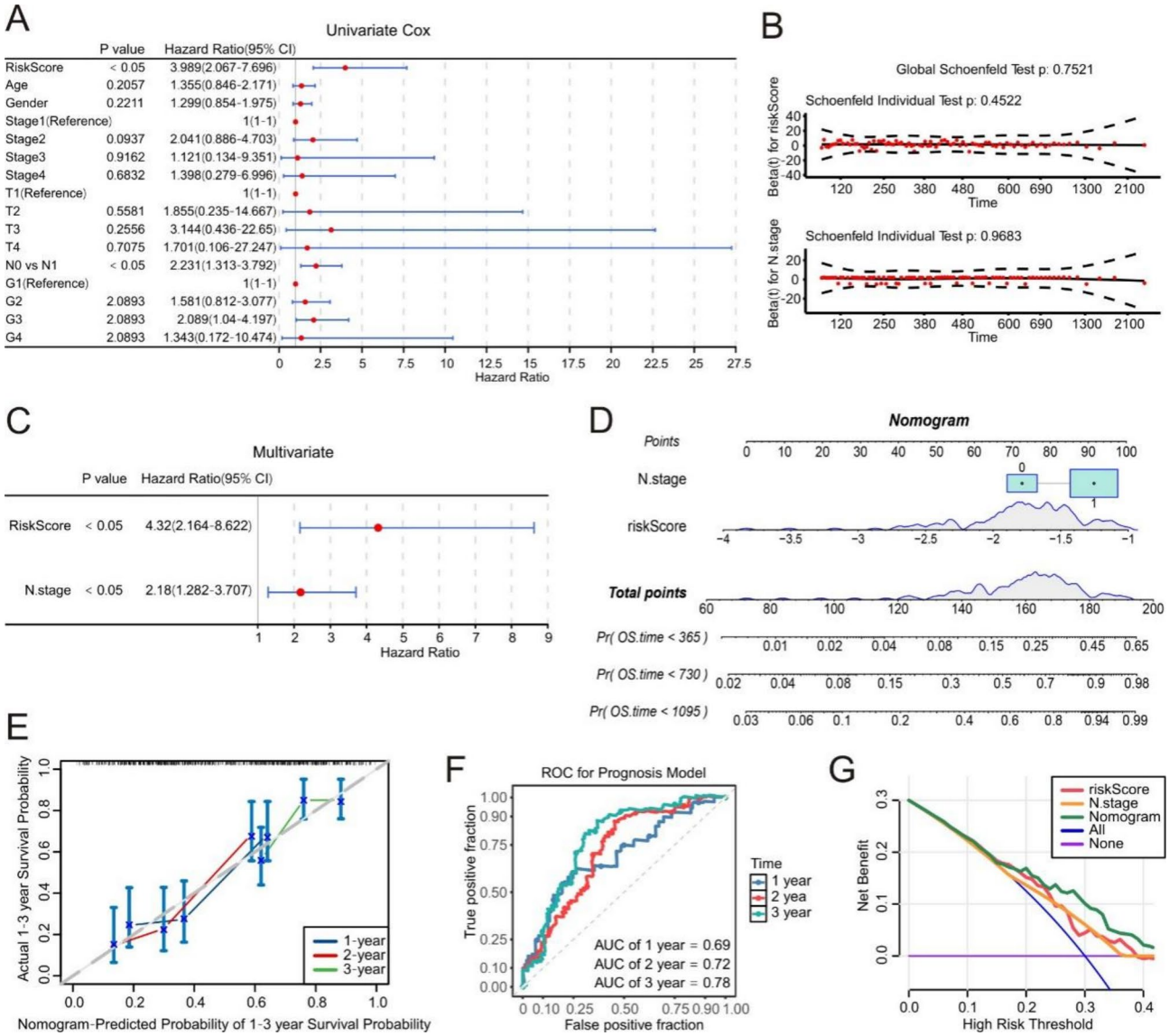

Fig. 5. Construction of a nomogram based on independent prognostic factors. (**A**) Clinicopathologic characteristics and risk modeling of patients in the training set univariate cox analysis of forest plots. (**B**) PH hypothesis test. (**C**) Clinicopathologic characteristics of training set patients and risk models for multifactorial cox analysis of forest plots. (**D**) Nomogram of multifactorial independent prognostic models. (**E**) Calibration curves for nomogram models. (**F**) ROC curves of nomogram. (**G**) DCA decision curve. The horizontal coordinate was the risk threshold and the vertical coordinate was the net benefit ratio.

probability of PC patients (Fig. 5C). Through a series of analyses, the N stage and risk score were determined to be independent prognostic factors for PC. Subsequently, a nomogram was developed that assigned specific point values to each independent prognostic factor. The total score, obtained by summing these points, indicated that higher scores were associated with increased mortality risk for PC patients (Fig. 5D). Calibration curves demonstrated a small deviation between the model predictions and the actual results (Fig. 5E). Moreover, the nomogram achieved AUC values exceeding 0.6 for 1-, 2-, and 3-year predictions (Fig. 5F), indicating robust predictive performance. The DCA revealed that the nomogram provided a greater net benefit compared to individual factors alone (Fig. 5G). Overall, these results validated the nomogram's strong capability in predicting mortality for PC patients, establishing it as a valuable tool for personalized risk assessment and management in clinical practice.

Deciphering the differences of functional pathways and mutation status between two risk cohorts

GSEA analysis identified that two risk cohorts were significantly enriched in 26 KEGG pathways. The top five pathways with the highest enrichment scores included "Type II diabetes mellitus", "calcium signaling pathway", "cell cycle", "spliceosome", and "neuroactive ligand-receptor interaction" (Fig. 6A). In high-risk cohorts, the three

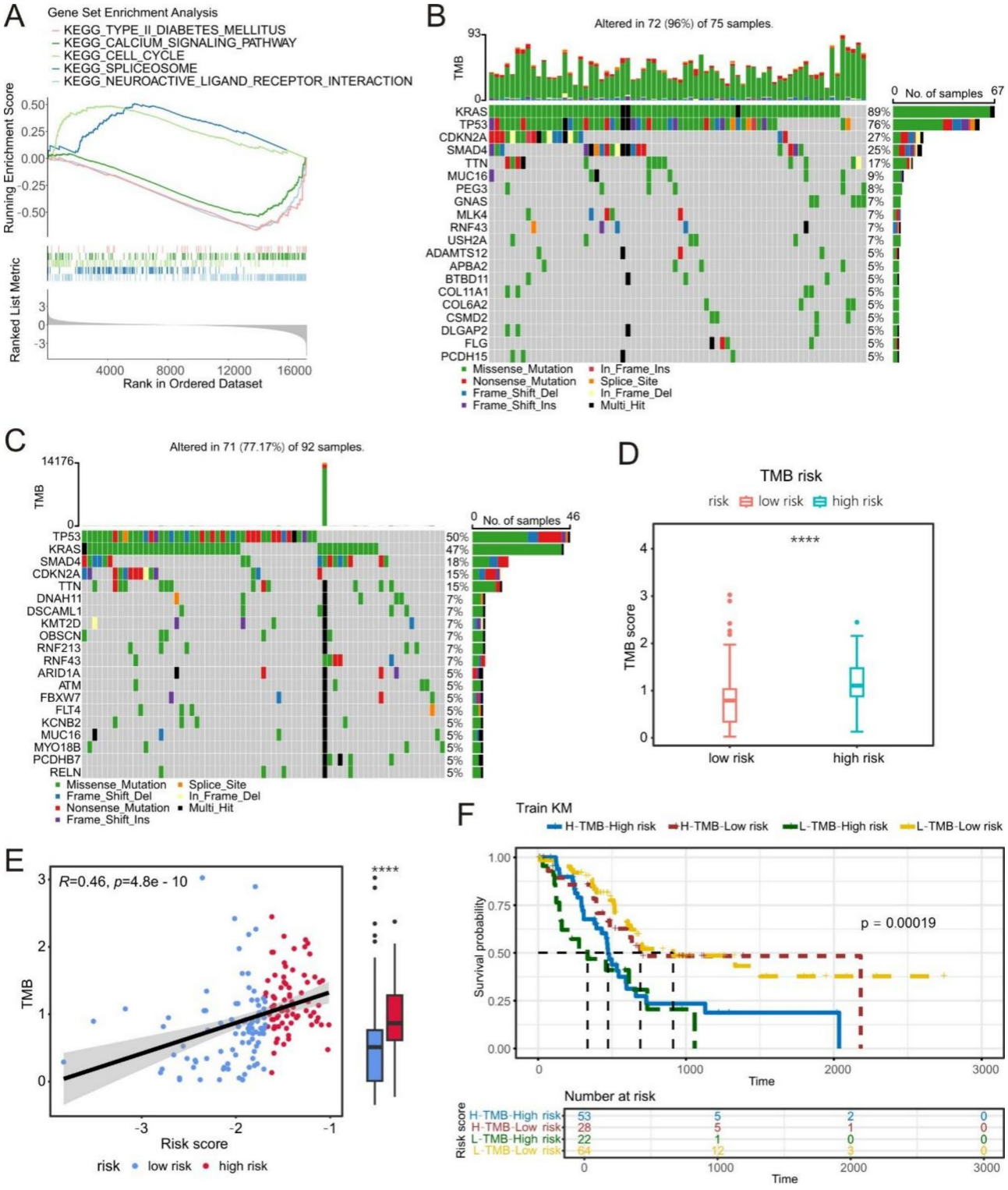

Fig. 6. GSEA enrichment and tumor mutation analysis. (**A**) GSEA enrichment results for low and high risk groups. Each line represents a pathway. (**B**) Tumor somatic mutations in the high-risk group, with different colors indicating mutation types and a bar graph showing the total number of mutations. (**C**) Tumor somatic mutations in the lower-risk group, with different colors representing mutation types and a bar graph showing the total mutation count. (**D**) TMB scores in patients with high-risk and low-risk PC. (**E**) Differences in tumor somatic mutations between low- and high-risk groups. (**F**) K–M curves for low and high TMB groups in Training set TCGA-PAAD.

genes with the highest mutation frequencies were KRAS (89%), TP53 (76%), and CDKN2A (27%) (Fig. 6B). In contrast, low-risk cohorts showed the highest mutation frequencies for TP53 (50%), KRAS (47%), and SMAD4 (18%) (Fig. 6C). The predominant mutation types included missense mutations, nonsense mutations, and multi-hit. Moreover, high-risk PC patients exhibited significantly higher TMB scores ($P < 0.05$) compared to low-risk patients (Fig. 6D). Spearman correlation analysis indicated a strong positive relationship between risk score and TMB score (cor = 0.46, $P = 6.3 \times 10^{-10}$) (Fig. 6E). In addition, K–M survival analysis revealed significant differences among the four groups ($P = 0.00019$) (Fig. 6F). Notably, PC patients in the H-TMB + low-risk group had a higher survival probability than those in the H-TMB + high-risk group ($P = 0.04$). Additionally, patients in the L-TMB + low-risk group demonstrated better survival rates compared to the H-TMB + high-risk group ($P = 0.00062$). Furthermore, individuals in the H-TMB + low-risk group had improved survival odds over those in the L-TMB + high-risk group ($P = 0.018$), while L-TMB + low-risk patients fared better than L-TMB + high-risk patients ($P = 0.00017$) (Supplementary Fig. 4). These findings highlight potential strategies for targeted therapies and personalized treatment in PC management.

Investigating the therapeutic effect of immunotherapy on PC

The Fig. 7A illustrates the expression levels of 20 immunosuppressive factors. The analysis revealed that PVRL2 had the strongest direct relationship with the risk score, while CD160 demonstrated the highest negative correlation (cor = − 0.51, $P < 0.05$) (Fig. 7B, Supplementary Table 5). Additionally, a heatmap displaying the expression of 38 immunosuppressive factors was presented in Fig. 7C. Here, CD276 showed the highest positive correlation with the risk score (cor = 0.431, $P < 0.05$), whereas IL6R had the highest negative correlation (cor = − 0.516, $P < 0.05$) (Fig. 7D, Supplementary Table 6). Furthermore, Fig. 7E presents the expression of 36 chemotactic factors, where CCL20 displayed the highest positive correlation with the risk score (cor = 0.32, $P < 0.05$), and CCL14 had the highest negative correlation (cor = − 0.551, $P < 0.05$) (Fig. 7F, Supplementary Table 7). These results underscored the complex interplay between immune factors and risk scores, highlighting their potential significance in tumor biology and PC patient's prognosis.

Revealing differences of drug sensitivity in high- and low-risk cohorts

The drug sensitivity analysis revealed that 129 drugs exhibited significant differences in IC_{50} values between the two risk cohorts ($P < 0.05$). The top 10 drugs identified were AG.014699, BI.2536, Cyclopamine, EHT.1864, FH535, Gemcitabine, Rapamycin, Roscovitine, VX.680, and WZ.1.84. Notably, AG.014699, BI.2536, Gemcitabine, Roscovitine, VX.680, and WZ.1.84 showed significantly reduced IC50 values in the high-risk cohort, suggesting increased drug sensitivity in these patients. Conversely, Cyclopamine, EHT.1864, FH535, and Rapamycin displayed markedly higher IC_{50} values in the high-risk cohort, suggesting that these patients had reduced sensitivity to these drugs (Fig. 8A). Additionally, the 3D conformations of the eight drugs were presented (the conformations of FH535 and Rapamycin were not found) (Fig. 8B). These findings suggested that the differential drug sensitivities observed between risk cohorts might inform personalized treatment strategies, potentially allowing for more effective selection of therapies based on individual patient risk profiles.

Exploring the expression of biomarkers in clinical samples

Gene expression analysis in the GSE62452 dataset revealed that the expression of ADH1A, ACACB, CD36, CERS4, PDE3B, and CRAT was obviously lower in tumor samples, while the expression of ALOX5 was markedly higher in tumor samples (Fig. 9A). Notably, RT-qPCR results further supported these findings, with ADH1A ($p = 0.025$), ACACB ($p = 0.021$), CD36 ($p = 0.01$), CERS4 ($p = 0.005$), PDE3B ($p < 0.0001$), and CRAT ($p = 0.03$) showing significantly reduced expression in tumor tissues, whereas ALOX5 exhibited significantly elevated expression in tumor samples ($p < 0.001$) (Fig. 9B). This comprehensive analysis highlighted expression of biomarkers that could guide personalized treatment strategies for PC patients.

Discussion

PC remains one of the deadliest malignancies globally, with metastatic disease present in approximately half of newly diagnosed cases[50–52]. Despite surgical resection being the only potentially curative option, current therapeutic strategies benefit only about 20% of patients[52]. This critical situation underscores the need for novel biomarkers to predict the prognosis of PC patients and to develop personalized treatment strategies[22,23]. Prior studies have identified potential risk markers such as PYGL, CCND2, BCAT1 and KRT7[53,54]. Although many risk markers have been developed to predict prognosis, their sensitivity and specificity remain unsatisfactory. Given the pivotal roles of macrophages and lipid metabolism in PC carcinogenesis and progression[49,55], this study identified biomarkers associated with MRGs and LMRGs in PC and constructed a prognostic model based on biomarkers through comprehensive analyses using the TCGA and GEO public databases. Notably, this model serves as an independent prognostic indicator. Additionally, we developed a nomogram that incorporates both clinical information and prognostic scores to enhance the clinical utility of this model, which was validated through calibration curves, ROC curves, and DCA curves. Collectively, these findings suggest that the MRGs-LMRGs-based prognostic model holds significant potential for prognostication in PC and could offer valuable insights for personalized treatment strategies.

Through intersecting analysis, we identified 38 candidate genes, which were primarily associated with lipid and fatty acid metabolic pathways, this was confirmed by GO and KEGG enrichment analysis. Further investigations highlighted seven specific biomarkers, including six upregulated genes in the normal group—ADH1A, ACACB, CD36, CERS4, PDE3B, and CRAT—and one downregulated gene in the normal group, ALOX5. Survival analysis indicated that higher expression levels of ADH1A, ACACB, CD36, CERS4, PDE3B, and CRAT were correlated with improved patient outcomes, suggesting these markers could predict surgical

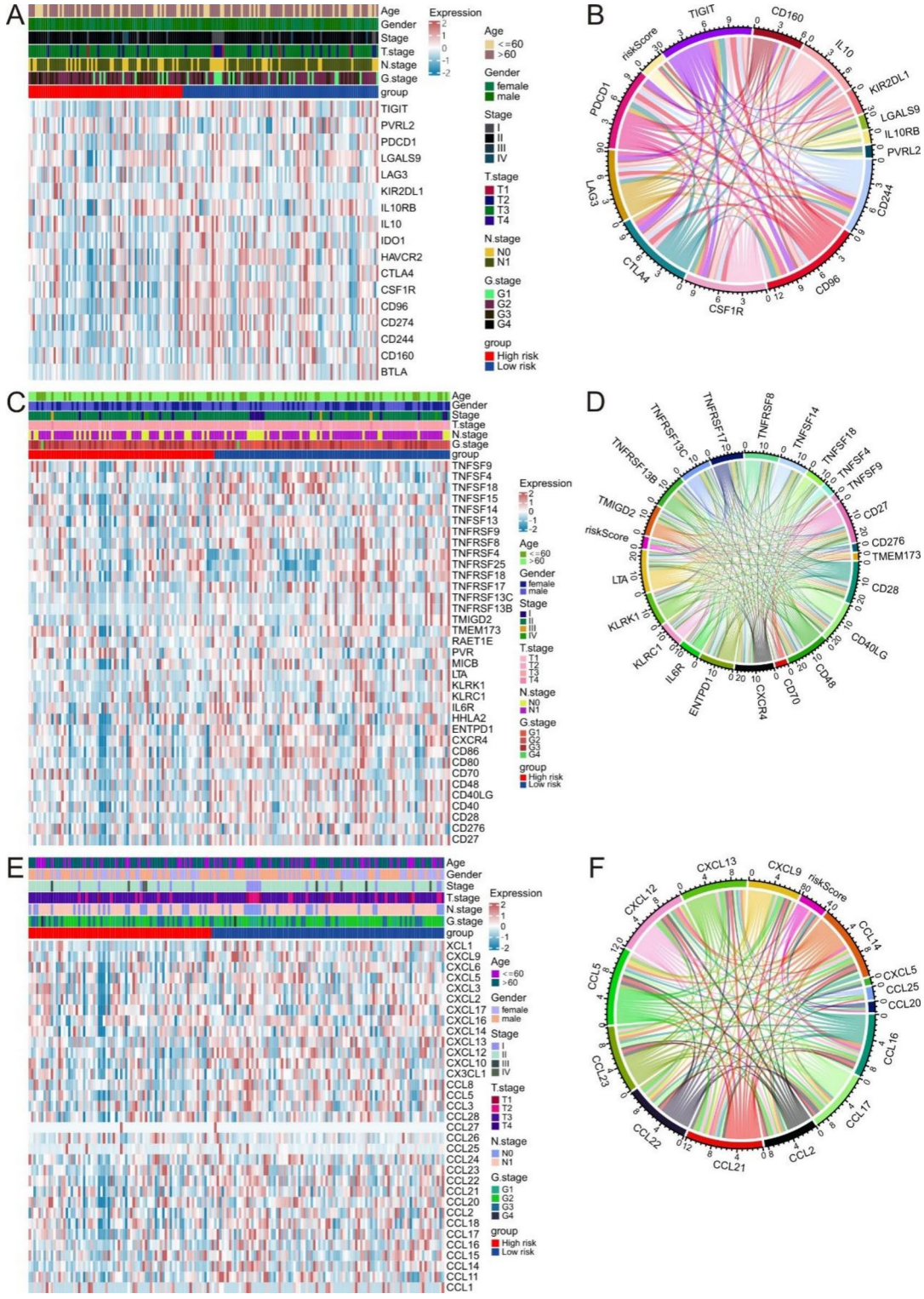

Fig. 7. Immunoscape and immune checkpoint analysis. (**A**) Expression of immunosuppressive factors between low and high risk groups. (**B**) Correlation between immunosuppressive factors and risk scores. (**C**) Expression of immune activating factors between low and high risk groups. (**D**) Correlation between immune activating factors and risk scores. (**E**) Expression of chemokines between low and high risk groups. (**F**) correlation between chemokines and risk scores.

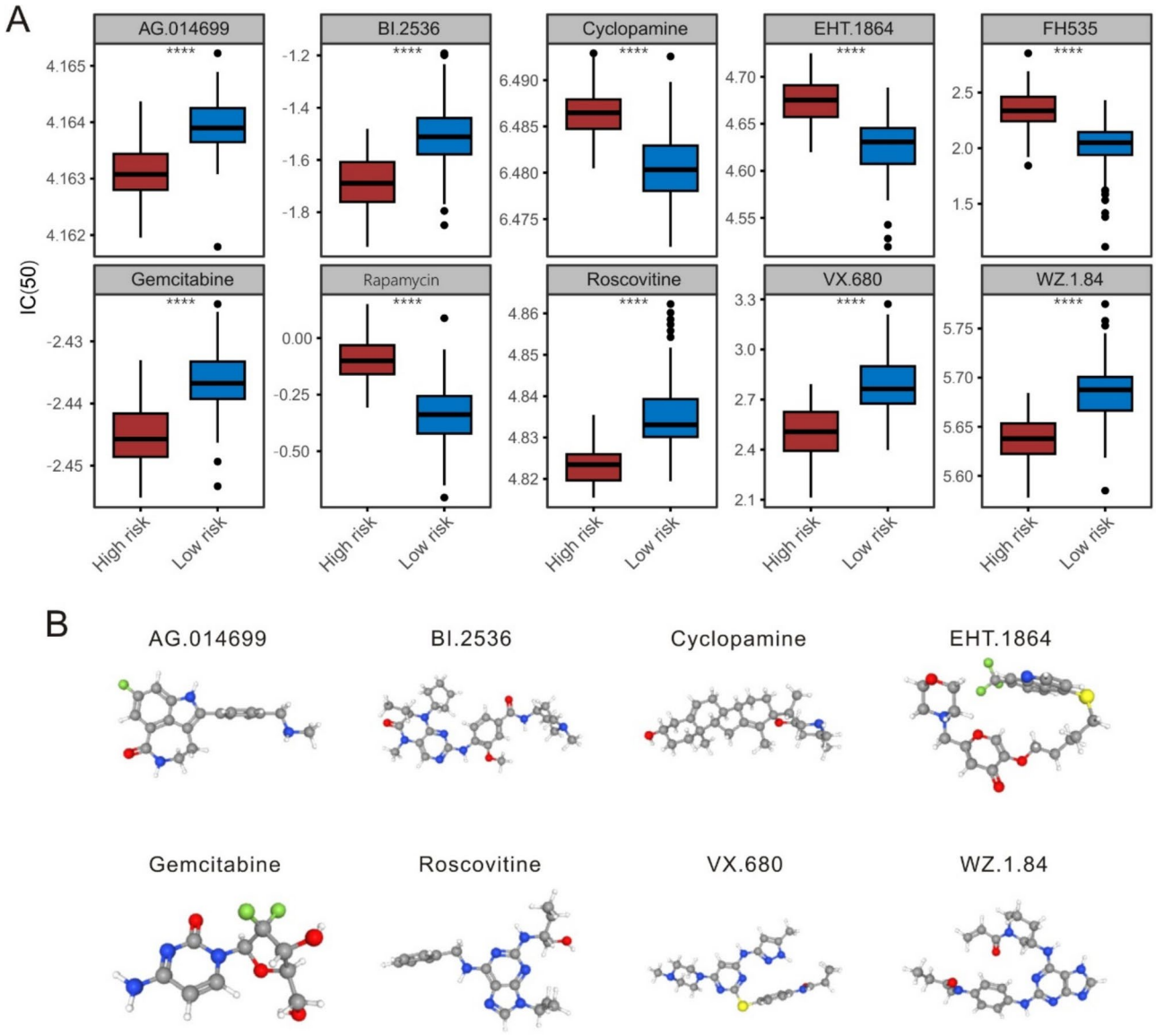

Fig. 8. Drug sensitivity analysis. (**A**) Analysis of differences in IC50 of corresponding drugs between low and high risk groups. ****, $P < 0.0001$. (**B**) Three-dimensional conformations of corresponding drugs in the Pubchem database.

treatment efficacy. Conversely, patients with elevated ALOX5 expression had poorer prognoses, indicating the need for alternative therapeutic strategies and further research.

Among these seven genes, ALOX5 was found to be highly expressed in PC and demonstrated independent prognostic value concerning overall survival (OS)[56]. ALOX5, as part of the lipoxygenase family, primarily mediates arachidonic acid metabolism to produce leukotrienes[57]. In immune regulation, ALOX5 promotes PC invasion and metastasis by modulating M2 polarization of tumor-associated macrophages[56]. Its low expression correlates with poor survival in prostate cancer[58], while overexpression exacerbates lung cancer progression via upregulating matrix metalloproteinase 9 (MMP9) expression[59]. Although ALOX5 is considered a tumor-promoting factor in pancreatic cancer, its role seems to be contradictory in other cancers, such as prostate cancer. In prostate cancer, low expression of ALOX5 is associated with poor survival, suggesting that it may have a tumor-suppressive effect[60]. This difference may be attributed to the variations in the tumor microenvironment and signaling pathways among different cancer types.In pancreatic cancer, ALOX5 promotes tumor progression by regulating the M2 polarization of tumor-associated macrophages (TAMs) and enhancing the production of leukotrienes. Leukotrienes are known to contribute to tumor invasion and metastasis[56]. Specifically, ALOX5 promotes the M2 polarization of TAMs through the JAK/STAT signaling pathway, thereby inhibiting the anti-tumor immune response. It also enhances the invasiveness and metastatic ability of tumor cells through metabolites such as leukotriene B4 (LTB4). In contrast, in prostate cancer, ALOX5 may exert an anti-tumor effect by participating in the regulation of lipid metabolism and inflammatory responses, thus suppressing tumor growth[60]. Such tissue-specific functional differences suggest that the tumor-promoting effect of ALOX5

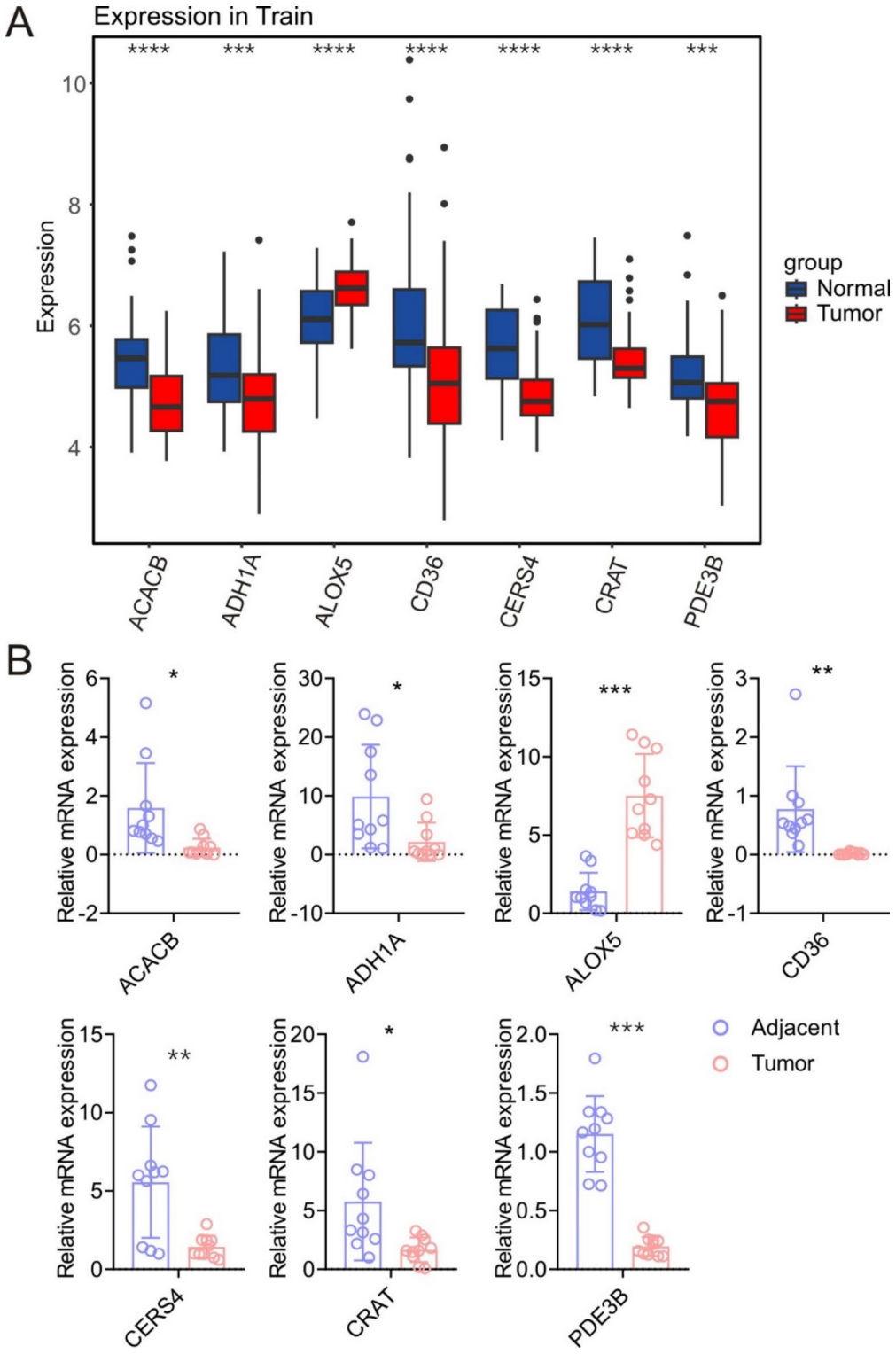

Fig. 9. Expression validation of prognostic genes. (**A**) Expression of prognostic genes in the training set GSE62452. (**B**) Prognostic gene expression level in tissue samples of PC patients. $^{*}P<0.05$, $^{**}P<0.01$, $^{***}P<0.001$, $^{****}P<0.0001$.

in pancreatic cancer may be closely related to its unique tumor microenvironment. Future research should further explore the specific molecular mechanisms of ALOX5 in pancreatic cancer to develop targeted treatment strategies.

ADH1A participates in fatty acid metabolism and counteracts lipid peroxidation[61]. Previous studies have shown that overexpression of ADH1A in gastric cancer cells suppresses proliferation, migration, and invasion

by modulating the cGMP/PKG signaling pathway and inflammatory cytokines such as IL-6 and IFN-γ[62]. Our study aligns with these findings as we observe significantly reduced ADH1A expression in pancreatic tumor tissues. High ADH1A expression is associated with increased chemotherapy sensitivity and higher infiltration of CD4+ T cells, CD8+ T cells, and macrophages in the tumor microenvironment, indicating a protective role in Pancreatic Ductal Adenocarcinoma (PDAC) tissues[63,64].

CERS4, a key enzyme in ceramide synthesis, is closely linked to pathways involving cell death and proliferation[65,66]. In colorectal cancer patients, CERS4 expression is significantly downregulated, with T cells lacking CERS4 exhibiting sustained activation and inhibited inflammation resolution, leading to increased tumor burden in a colitis-associated cancer mouse model[67]. Conversely, high CERS4 expression is correlated with better prognostic outcomes in non-small cell lung cancer[68].

PDE3B, responsible for degrading intracellular cyclic adenosine monophosphate (cAMP) and cyclic guanosine monophosphate (cGMP), shows reduced expression in bladder cancer, correlating with better prognosis[69]. Additionally, research has found that circ_PDE3B is highly expressed in esophageal squamous cell carcinoma tissues and cells, where knocking down circ_PDE3B significantly reduces cell proliferation, migration, and invasion by regulating miR-136-5p and MAP3K2[70]. In Sa3 and HeLa cells, knocking down PDE3B induces an increase in cyclic GMP, thereby inhibiting tumor cell growth[71]. Thus, the specific role of PDE3B in PC warrants further investigation.

CrAT, mainly located in the mitochondrial matrix, catalyzes transfer reactions between carnitine and acetyl-CoA[72]. Existing research links CrAT with melanoma, suggesting that through fatty acid metabolism, it might influence tumor cell migration and invasion[73]. However, more experimental evidence is needed to clarify its specific mechanisms in PC.

ACACB plays a critical role in maintaining the balance between fatty acid synthesis and oxidation[74]. Although its specific mechanisms in PC are still under investigation, existing clues suggest that ACACB may impact cancer cell proliferation and survival strategies by regulating fatty acid metabolism[75,76].

Recent studies using bioinformatics and systems biology approaches have revealed the crucial roles of macrophages and lipid metabolism in cancer progression. A study on the impact of dermatomyositis on interstitial lung disease[77] found that the NF-κB signaling pathway regulates macrophage activation, providing an analogical perspective on macrophage behavior in the tumor microenvironment. Research on type 2 diabetes and non-alcoholic fatty liver disease[78] has clarified the significance of abnormal lipid metabolism in these diseases. The lipid metabolism pathways involved have potential links to lipid metabolism reprogramming in cancer. These findings offer new evidence for understanding metabolic disorders in tumors such as pancreatic cancer and developing targeted therapeutic strategies.

In this study, Gene Set Enrichment Analysis (GSEA) showed that the "cell cycle" pathway was significantly enriched in both the high-risk and low-risk cohorts. This result suggests that the activation of the cell cycle may play an important role in the progression of pancreatic cancer (PC), and there may be an interaction between it and the regulation of lipid metabolism and macrophages. Recent studies have shown that lipid metabolism plays a crucial role in regulating the cell cycle. For example, fatty acid synthase (FASN), a key enzyme for de novo fatty acid synthesis, is upregulated in various cancers, including pancreatic cancer[79]. High levels of FASN increase the synthesis of fatty acids, which can be used for cell membrane biosynthesis and energy production, thus promoting the progression of the cell cycle[80]. In pancreatic cancer cells, enhanced lipid metabolism can promote the expression of cell cycle regulators (such as cyclin D1), and cyclin D1 is crucial for the transition of the cell cycle from the G1 phase to the S phase[81]. Macrophages, especially tumor-associated macrophages (TAMs), are also closely related to the cell cycle. In the tumor microenvironment, TAMs polarize into the M2 phenotype, and the cytokines and growth factors secreted by these M2 macrophages can directly affect the cell cycle of cancer cells[82]. For example, M2 macrophages secrete a large amount of CCND1 and CCNE1, which are key regulators of the cell cycle. These factors can prompt pancreatic cancer cells to enter the cell cycle and enhance their proliferative ability[26]. In addition, lipid metabolism can regulate the polarization of macrophages. Oxidized low-density lipoprotein (oxLDL) can induce macrophages to polarize into the M2 phenotype[55]. Once polarized, M2 macrophages can further promote the activation of the cell cycle in cancer cells, forming a positive feedback loop that may drive the progression of pancreatic cancer.In conclusion, the enrichment of the "cell cycle" pathway in our study may be closely related to the dysregulation of lipid metabolism and the polarization state of macrophages in pancreatic cancer. Further research is needed to fully elucidate the detailed molecular mechanisms behind these interactions.

We found that the mutation frequency of TP53 in the high-risk group was significantly higher than that in the low-risk group (76% vs. 50%). As a classical tumor suppressor gene, mutations in TP53 are closely associated with tumor invasiveness, metastasis, and therapeutic resistance in various cancers. Mutations in TP53 not only lead to the loss of its tumor suppressor function but may also promote tumor progression by affecting key pathways such as cell cycle regulation, DNA repair, and apoptosis[83]. Especially in pancreatic cancer, TP53 mutations, in conjunction with KRAS mutations, drive the metabolic reprogramming and immune evasion of tumor cells[84]. Our Gene Set Enrichment Analysis (GSEA) showed that the high-risk group was significantly enriched in the "cell cycle" pathway, which is highly consistent with the function of TP53 mutations. The normal function of TP53 is to regulate the cell cycle checkpoints to prevent cells with DNA damage from entering the proliferative cycle. However, TP53 mutations can lead to the loss of control of the cell cycle and promote the abnormal proliferation of tumor cells[85]. In addition, TP53 mutations may further exacerbate the metabolic disorders of tumor cells by affecting the expression of genes related to lipid metabolism. For example, TP53 mutations have been shown to upregulate the expression of fatty acid synthase (FASN), promoting lipid synthesis in tumor cells, thereby supporting their rapid proliferation and survival[8,86].Therefore, the difference in the mutation frequency of TP53 not only reflects that the tumors of patients in the high-risk group are more invasive but may also reduce the sensitivity of these patients to traditional chemotherapy and targeted therapies by affecting the cell cycle

and metabolic pathways. Future research could further explore how TP53 mutations affect the progression of pancreatic cancer and the therapeutic response by regulating these pathways, thus providing a theoretical basis for the development of personalized treatment strategies targeting TP53 mutations.

Besides macrophages and lipid metabolism-related biomarkers, our study also identified the correlation between immune response and risk scores based on immune-related genes and more effective guidance for PC immunotherapy. Immunosuppressive factors include PVRL2, CD160, CD276, and CCL20. PVRL2 showed the strongest positive correlation with the risk score (cor = 0.356, $p < 0.05$) in the present study. It is known to promote tumor growth by inhibiting CD8+ T cells and NK cells, playing a critical role in creating an immunosuppressive environment[87], especially in liver cancer, where its expression is significantly upregulated. Blocking PVRL2 enhances immune cell-induced tumor lysis[88]. CD160 is an Ig-like glycoprotein acting as an activating receptor on lymphocytes[89]. In hepatocellular carcinoma, lower densities of intratumoral CD160+ cells correlate with more severe disease and higher recurrence rates[90]. Our study found CD160 to have a strong negative correlation with the risk score (cor = − 0.51, $p < 0.05$), indicating that the expression of CD160 in PC may be associated with better prognosis. Therefore, comprehensive consideration of the expression of these immune-related markers is helpful to optimize the treatment strategy of PC.

CD276 is an immune checkpoint protein with high expression linked to lower survival in PC[91,92]. CAR-T cells targeting CD276 have shown high cytotoxicity against various human cancer cell lines, including pancreatic, liver, glioma, renal, fibrosarcoma, breast, ovarian, and colon cancers[93]. In a study of 150 PC patients, high CD276 expression was prevalent in most tumor tissues and was independently associated with lower survival rates[94]. Aligned with these findings, our results revealed a significant direct correlation between CD276 and the risk score (cor = 0.431, $p < 0.05$).

Chemokines are crucial regulators of tumor progression, involved in controlling apoptosis, migration, proliferation, invasion, and metastasis of tumor cells[95]. CCL20 is a protein expressed in the liver, colon, and skin, playing roles in inflammation and homeostasis through its specific receptor, CCR6[96]. The CCR6/CCL20 axis has been shown to aid tumor growth and liver metastasis in PC mouse models[97]. In alignment with these findings, our immune landscape analysis revealed a strong positive correlation between CCL20 and the risk score (cor = 0.32, $p < 0.05$). Additionally, CCL14 has been shown to inhibit colon cancer cell proliferation and invasion by promoting M1 macrophage polarization and suppressing M2 polarization[98]. In our study, we found that CCL14 had the strongest negative correlation with the PC risk score (cor = − 0.551, $p < 0.05$).

In addition, the biomarkers identified in this study, such as ALOX5 and ADH1A, have significant potential in being integrated into the current treatment strategies for pancreatic cancer (PC). For ALOX5, it is highly expressed in pancreatic cancer and is associated with a poor prognosis. In the current treatment strategies, it is advisable to consider incorporating ALOX5 inhibitors into the treatment regimen. Existing studies have shown that ALOX5 is involved in the arachidonic acid metabolic pathway, promoting the invasion and metastasis of tumor cells[99]. For example, zileuton, as an ALOX5 inhibitor, has demonstrated the effects of inhibiting tumor growth and metastasis in preclinical studies of some cancers[100]. In the treatment of pancreatic cancer, for patients with high ALOX5 expression, the combined use of an ALOX5 inhibitor and traditional chemotherapeutic drugs (such as gemcitabine) may enhance the efficacy of chemotherapy by inhibiting the migration and invasion of tumor cells. At the same time, it can regulate the tumor microenvironment and improve the sensitivity to immunotherapy. ADH1A is downregulated in pancreatic cancer tissues, and its high expression is associated with increased chemosensitivity. To better integrate ADH1A into the treatment strategy, attempts can be made to develop drugs or therapies that can upregulate the expression of ADH1A. From a molecular mechanism perspective, ADH1A is involved in fatty acid metabolism and counteracts lipid peroxidation[101]. By screening small-molecule compounds or biological agents to activate the expression regulation pathway of ADH1A, there is hoped to improve the response of pancreatic cancer patients to chemotherapy. In addition, gene therapy strategies can also be considered as a potential option. By using vectors to introduce the ADH1A gene into tumor cells, the expression level can be restored, thereby enhancing the effect of chemotherapy[102]. In conclusion, the rational integration of biomarkers such as ALOX5 and ADH1A into the treatment strategies for pancreatic cancer is expected to provide more effective personalized treatment options for pancreatic cancer patients and improve their prognosis.

In this study, the drug sensitivity analysis showed that drugs such as AG.014699, BI.2536, and Gemcitabine exhibited lower IC50 values in high-risk pancreatic cancer patients, indicating that these drugs may have higher efficacy for high-risk patients. However, the clinical relevance of these drugs still needs further exploration. AG.014699 is a PARP inhibitor that has currently undergone clinical trials in multiple cancer types, especially demonstrating significant efficacy in BRCA mutation-related breast cancer and ovarian cancer[103]. Although there is relatively less research on PARP inhibitors in pancreatic cancer, existing studies have shown that PARP inhibitors may have potential therapeutic value in pancreatic cancer patients with DNA repair defects[104]. Particularly for high-risk pancreatic cancer patients, PARP inhibitors may enhance the efficacy of chemotherapeutic drugs by inhibiting the DNA repair pathway[105]. Gemcitabine is a standard first-line chemotherapeutic drug for pancreatic cancer and is widely used in clinical treatment[106]. Our research results further support the sensitivity of Gemcitabine in high-risk patients, suggesting its potential application value in personalized treatment.In addition, BI.2536 is a PLK1 inhibitor, and multiple clinical trials are currently underway to evaluate its efficacy in various solid tumors, including pancreatic cancer[107]. PLK1 plays a crucial role in cell cycle regulation, and inhibiting PLK1 may enhance the effect of chemotherapy by interfering with the proliferation and survival of tumor cells[108]. Although these drugs show potential sensitivity in high-risk pancreatic cancer patients, their clinical application still needs further verification. Future research should combine clinical trial data to evaluate the actual efficacy and safety of these drugs in pancreatic cancer patients, especially for personalized treatment regimens targeting high-risk patients.

Taken together, a comprehensive investigation of the discrepancies in immunosuppressive factors between high- and low-risk groups can assist in the identification of valuable immunotherapy targets, which can serve as a reference for clinicians in the development of a more tailored treatment plan for their patients.

However, this study still has some limitations. Firstly, the bioinformatics analysis relies on existing databases. The limited sample size may affect the generality and accuracy of the results. Moreover, the imbalance in the number of samples may lead to a decrease in the statistical power of the tests, causing the omission of key information or making the results of the differential expression analysis overly biased towards tumor samples. Secondly, in the analysis of the immune landscape, the correlations between the risk score and immune factors such as PVRL2 and CD276 lack in vitro or in vivo functional verification. Meanwhile, the sample size for RT-qPCR verification is relatively small (20 samples), which limits the universality of the results and the statistical power. In future research, the sample size will be expanded, and more patient samples from different ethnic groups, regions, and clinical backgrounds will be included. By integrating more clinical and pathological characteristics (such as tumor staging, molecular subtypes, etc.), the universality of the model and its clinical application value will be enhanced. At the same time, functional verification experiments are planned to be carried out. Gene editing technologies such as CRISPR/Cas9 will be used to regulate the expression of immune factors. Combined with animal models of pancreatic cancer, the role of immune factors in tumor progression and their causal relationships with the risk score will be explored. In addition, multi-omics data will be further integrated to optimize the prediction model, and the clinical application potential of the biomarkers will be verified through prospective clinical trials, providing a more solid theoretical foundation and practical basis for the personalized treatment of pancreatic cancer.

In conclusion, this study emphasizes the prognostic significance of MRGs and LMRGs in PC, uncovering novel biomarkers and potential therapeutic targets. As the understanding of PC biology deepens, these findings will assist in propelling personalized treatment advancements, ultimately improving patient survival outcomes.

From the perspective of clinical application, the biomarkers identified in this study provide a new direction for the selection of treatment regimens. For patients with high ALOX5 expression, since this biomarker is associated with tumor invasion and poor prognosis, ALOX5 inhibitors can be added to traditional treatments. By doing so, it can inhibit the migration and invasion of tumor cells, regulate the tumor microenvironment, and enhance the effectiveness of immunotherapy. For patients with low ADH1A expression, considering that its high expression is positively correlated with chemosensitivity, gene therapy can be attempted to increase its expression level, or small-molecule drugs that enhance its activity can be screened to improve the chemotherapeutic response of these patients and optimize the treatment effect.In terms of future research, it is necessary to verify the stability and predictive ability of the biomarkers in large-scale and diverse patient cohorts to ensure their reliability under different clinical backgrounds. In-depth basic research should be carried out to clarify the molecular regulatory mechanisms of these biomarkers in the occurrence and development of pancreatic cancer, laying a theoretical foundation for the development of precise targeted therapeutic drugs. Prospective clinical trials should be conducted to compare the advantages of personalized treatment based on biomarkers and traditional treatment in improving patients' quality of life and prolonging their survival, accelerating the transformation of research achievements into clinical practice.Through these clinical application plans and future research directions, the aim is to better apply the research achievements to clinical practice, provide more effective personalized treatment strategies for pancreatic cancer patients, and effectively enhance the practicality and clinical value of the research.

Data availability

The data underlying the results presented in this study are provided within the manuscript and its supplementary materials. To access the raw data, please contact the corresponding author with a reasonable request.

Received: 22 November 2024; Accepted: 17 April 2025
Published online: 25 April 2025

References

1. Hu, Z. I. & O'Reilly, E. M. Therapeutic developments in pancreatic cancer. *Nat. Rev. Gastroenterol. Hepatol.* **21**, 7–24 (2024).
2. Yin, X. et al. Lipid metabolism in pancreatic cancer: Emerging roles and potential targets. *Cancer Commun. (Lond)* **42**, 1234–1256 (2022).
3. Stoffel, E. M., Brand, R. E. & Goggins, M. Pancreatic cancer: Changing epidemiology and new approaches to risk assessment, early detection, and prevention. *Gastroenterology* **164**, 752–765 (2023).
4. Luo, X. et al. Emerging roles of lipid metabolism in cancer metastasis. *Mol. Cancer* **16**, 76 (2017).
5. Sunami, Y., Rebelo, A. & Kleeff, J. Lipid metabolism and lipid droplets in pancreatic cancer and stellate cells. *Cancers (Basel)* **10**, 3 (2017).
6. Ye, H. et al. Tumor-associated macrophages promote progression and the Warburg effect via CCL18/NF-kB/VCAM-1 pathway in pancreatic ductal adenocarcinoma. *Cell Death Dis.* **9**, 453 (2018).
7. Georgoudaki, A.-M. et al. Reprogramming tumor-associated macrophages by antibody targeting inhibits cancer progression and metastasis. *Cell Rep.* **15**, 2000–2011 (2016).
8. Currie, E., Schulze, A., Zechner, R., Walther, T. C. & Farese, R. V. Cellular fatty acid metabolism and cancer. *Cell Metab.* **18**, 153–161 (2013).
9. Zhang, R. et al. Oncogenic KRASG12D reprograms lipid metabolism by upregulating SLC25A1 to drive pancreatic tumorigenesis. *Cancer Res.* **83**, 3739–3752 (2023).
10. Carrer, A. et al. Acetyl-CoA metabolism supports multistep pancreatic tumorigenesis. *Cancer Discov.* **9**, 416–435 (2019).
11. Khwairakpam, A. D. et al. The vital role of ATP citrate lyase in chronic diseases. *J. Mol. Med. (Berl)* **98**, 71–95 (2020).
12. Zhou, T. et al. Serum low-density lipoprotein and low-density lipoprotein expression level at diagnosis are favorable prognostic factors in patients with small-cell lung cancer (SCLC). *BMC Cancer* **17**, 269 (2017).
13. Guillaumond, F. et al. Cholesterol uptake disruption, in association with chemotherapy, is a promising combined metabolic therapy for pancreatic adenocarcinoma. *Proc. Natl. Acad. Sci. U S A* **112**, 2473–2478 (2015).

14. Gallagher, E. J. et al. Elevated tumor LDLR expression accelerates LDL cholesterol-mediated breast cancer growth in mouse models of hyperlipidemia. *Oncogene* **36**, 6462–6471 (2017).
15. Morrison, A. H., Byrne, K. T. & Vonderheide, R. H. Immunotherapy and prevention of pancreatic cancer. *Trends Cancer* **4**, 418–428 (2018).
16. Pan, Y. et al. High-dimensional single-cell analysis unveils distinct immune signatures of peripheral blood in patients with pancreatic ductal adenocarcinoma. *Front. Endocrinol. (Lausanne)* **14**, 1181538 (2023).
17. Liu, J. et al. Tumoral EHF predicts the efficacy of anti-PD1 therapy in pancreatic ductal adenocarcinoma. *J. Exp. Med.* **216**, 656–673 (2019).
18. Lin, J., Lu, F., Wu, Y., Huang, H. & Pan, Y. The cellular trajectories of tumor-associated macrophages decipher the heterogeneity of pancreatic cancer. *Funct. Integr. Genomics* **23**, 343 (2023).
19. Chen, S. et al. Macrophages in immunoregulation and therapeutics. *Signal Transduct. Target. Ther.* **8**, 207 (2023).
20. Yan, J. & Horng, T. Lipid metabolism in regulation of macrophage functions. *Trends Cell Biol.* **30**, 979–989 (2020).
21. Yunna, C., Mengru, H., Lei, W. & Weidong, C. Macrophage M1/M2 polarization. *Eur. J. Pharmacol.* **877**, 173090 (2020).
22. Xiang, H. et al. Metabolic reprogramming of immune cells in pancreatic cancer progression. *Biomed. Pharmacother.* **157**, 113992 (2023).
23. Vassiliou, E. & Farias-Pereira, R. Impact of lipid metabolism on macrophage polarization: Implications for inflammation and tumor immunity. *Int. J. Mol. Sci.* **24**, 12032 (2023).
24. Pireaux, V. et al. Myeloperoxidase-oxidized LDLs enhance an anti-inflammatory M2 and antioxidant phenotype in murine macrophages. *Mediators Inflamm.* **2016**, 8249476 (2016).
25. de la Paz Sánchez-Martínez, M. et al. IL-17-differentiated macrophages secrete pro-inflammatory cytokines in response to oxidized low-density lipoprotein. *Lipids Health Dis.* **16**, 196 (2017).
26. Cao, Y. et al. Macrophages evoke autophagy of hepatic stellate cells to promote liver fibrosis in NAFLD mice via the PGE2/EP4 pathway. *Cell Mol. Life Sci.* **79**, 303 (2022).
27. Song, M., Chan, A. T. & Sun, J. J. E. Influence of the gut microbiome, diet, and environment on risk of colorectal cancer. *Gastroenterology* **158**, 322–340 (2020).
28. Li, J. et al. Lipid metabolism gene-wide profile and survival signature of lung adenocarcinoma. *Lipids Health Dis.* **19**, 222 (2020).
29. Sturm, G., Finotello, F. & List, M. Immunedeconv: An R package for unified access to computational methods for estimating immune cell fractions from bulk RNA-sequencing data. *Methods Mol. Biol.* **2120**, 223–232 (2020).
30. Subramanian, A. et al. Gene set enrichment analysis: a knowledge-based approach for interpreting genome-wide expression profiles. *Proc. Natl. Acad. Sci. U S A* **102**, 15545–15550 (2005).
31. Langfelder, P. & Horvath, S. WGCNA: An R package for weighted correlation network analysis. *BMC Bioinform.* **9**, 559 (2008).
32. Gustavsson, E. K., Zhang, D., Reynolds, R. H., Garcia-Ruiz, S. & Ryten, M. ggtranscript: An R package for the visualization and interpretation of transcript isoforms using ggplot2. *Bioinformatics* **38**, 3844–3846 (2022).
33. Gu, Z. & Hübschmann, D. Make interactive complex heatmaps in R. *Bioinformatics* **38**, 1460–1462 (2022).
34. Jia, A., Xu, L. & Wang, Y. Venn diagrams in bioinformatics. *Brief. Bioinform.* **22**, bbab108 (2021).
35. Yu, G., Wang, L.-G., Han, Y. & He, Q.-Y. clusterProfiler: An R package for comparing biological themes among gene clusters. *OMICS* **16**, 284–287 (2012).
36. Kanehisa, M., Furumichi, M., Sato, Y., Matsuura, Y. & Ishiguro-Watanabe, M. KEGG: Biological systems database as a model of the real world. *Nucleic Acids Res.* **53**, D672–D677 (2025).
37. Kanehisa, M. & Goto, S. KEGG: Kyoto encyclopedia of genes and genomes. *Nucleic Acids Res.* **28**, 27–30 (2000).
38. Shannon, P. et al. Cytoscape: A software environment for integrated models of biomolecular interaction networks. *Genome Res* **13**, 2498–2504 (2003).
39. Liu, T.-T. et al. Identification of CDK2-related immune forecast model and ceRNA in lung adenocarcinoma, a pan-cancer analysis. *Front. Cell Dev. Biol.* **9**, 682002 (2021).
40. Engebretsen, S. & Bohlin, J. Statistical predictions with glmnet. *Clin. Epigenetics* **11**, 123 (2019).
41. Zhang, S. et al. Development and validation of PET/CT-based nomogram for preoperative prediction of lymph node status in esophageal squamous cell carcinoma. *Ann. Surg. Oncol.* **30**, 7452–7460 (2023).
42. Sachs, M. C. plotROC: A tool for plotting ROC curves. *J. Stat. Softw.* **79**, 1–19 (2017).
43. Harrell, F. E., Jr. *Regression Modeling Strategies* 2nd edn (Springer, 2015).
44. Liu, S. et al. Three differential expression analysis methods for RNA sequencing: limma, EdgeR, DESeq2. *J. Vis. Exp.* **175**, e62528 (2021).
45. Mayakonda, A., Lin, D.-C., Assenov, Y., Plass, C. & Koeffler, H. P. Maftools: Efficient and comprehensive analysis of somatic variants in cancer. *Genome Res.* **28**, 1747–1756 (2018).
46. Robles-Jimenez, L. E. et al. Worldwide traceability of antibiotic residues from livestock in wastewater and soil: A systematic review. *Animals (Basel)* **12**, 60 (2021).
47. Gu, X. et al. Hub genes, diagnostic model, and predicted drugs related to iron metabolism in Alzheimer's disease. *Front. Aging Neurosci.* **14**, 949083 (2022).
48. Wang, W. et al. The cuproptosis-related signature associated with the tumor environment and prognosis of patients with glioma. *Front. Immunol.* **13**, 998236 (2022).
49. Hou, Z. et al. Loss of Annexin A1 in macrophages restrains efferocytosis and remodels immune microenvironment in pancreatic cancer by activating the cGAS/STING pathway. *J. Immunother. Cancer* **12**, 1929–1946 (2024).
50. Ansari, D. et al. Pancreatic cancer: Yesterday, today and tomorrow. *Fut. Oncol.* **12**, 1929–1946 (2016).
51. Goral, V. Pancreatic cancer: Pathogenesis and diagnosis. *Asian Pac. J. Cancer Prev.* **16**, 5619–5624 (2015).
52. Advancing on pancreatic cancer. *Nat. Rev. Gastroenterol. Hepatol.* **18**, 447 (2021).
53. Du, Y. et al. Integration of single-cell RNA sequencing and bulk RNA sequencing reveals that TAM2-driven genes affect immunotherapeutic response and prognosis in pancreatic cancer. *Int. J. Mol. Sci.* **24**, 12787 (2023).
54. Song, J. et al. Construction of a novel model based on cell-in-cell-related genes and validation of KRT7 as a biomarker for predicting survival and immune microenvironment in pancreatic cancer. *BMC Cancer* **22**, 894 (2022).
55. Bonilla, M. E. et al. Metabolic landscape of the healthy pancreas and pancreatic tumor microenvironment. *JCI Insight* **9**, e180114 (2024).
56. Hu, W.-M. et al. The ALOX5 inhibitor Zileuton regulates tumor-associated macrophage M2 polarization by JAK/STAT and inhibits pancreatic cancer invasion and metastasis. *Int. Immunopharmacol.* **121**, 110505 (2023).
57. Mashima, R. & Okuyama, T. The role of lipoxygenases in pathophysiology; new insights and future perspectives. *Redox Biol.* **6**, 297–310 (2015).
58. Liu, T. et al. ALOX5 deficiency contributes to bladder cancer progression by mediating ferroptosis escape. *Cell Death Dis.* **14**, 800 (2023).
59. Han, L. et al. Cancer-educated neutrophils promote lung cancer progression via PARP-1-ALOX5-mediated MMP-9 expression. *Cancer Biol. Med.* **21**, 175–192 (2024).
60. Dave, A. et al. Long-term dietary consumption of grapes affects kidney health in C57BL/6J mice. *Nutrients* **16**, 2309 (2024).
61. Boffetta, P. & Hashibe, M. Alcohol and cancer. *Lancet Oncol.* **7**, 149–156 (2006).
62. Ma, J., Shi, Y., Lu, Q. & Huang, D. Inflammation-related gene ADH1A regulates the polarization of macrophage M1 and influences the malignant progression of gastric cancer. *J. Inflamm. Res.* **17**, 4647–4665 (2024).

63. Pu, N. et al. Identification of an immune-related BAT signature for predicting adjuvant chemotherapy response and overall survival in patients with resected ductal adenocarcinoma of the pancreas. *J. Gastrointest. Surg.* **26**, 869–886 (2022).
64. Liao, X. et al. Distinct prognostic values of alcohol dehydrogenase mRNA expression in pancreatic adenocarcinoma. *Onco Targets Ther.* **10**, 3719–3732 (2017).
65. Chen, J. et al. Ceramide synthase-4 orchestrates the cell proliferation and tumor growth of liver cancer in vitro and in vivo through the nuclear factor-κB signaling pathway. *Oncol. Lett.* **14**, 1477–1483 (2017).
66. Fan, S.-H. et al. CERS2 suppresses tumor cell invasion and is associated with decreased V-ATPase and MMP-2/MMP-9 activities in breast cancer. *J. Cell Biochem.* **116**, 502–513 (2015).
67. El-Hindi, K. et al. T-cell-specific CerS4 depletion prolonged inflammation and enhanced tumor burden in the AOM/DSS-induced CAC model. *Int. J. Mol. Sci.* **23**, 1866 (2022).
68. Wang, J. et al. CERS4 predicts positive anti-PD-1 response and promotes immunomodulation through Rhob-mediated suppression of $CD8^+$ $Tim3^+$ exhausted T cells in non-small cell lung cancer. *Pharmacol. Res.* **194**, 106850 (2023).
69. Feng, Y. et al. PDE3B regulates KRT6B and increases the sensitivity of bladder cancer cells to copper ionophores. *Naunyn Schmiedebergs Arch. Pharmacol.* **397**, 4911–4925 (2024).
70. Yue, W. et al. CircRNA PDE3B regulates tumorigenicity via the miR-136-5p/MAP3K2 axis of esophageal squamous cell carcinoma. *Histol. Histopathol.* **38**, 1029–1041 (2023).
71. Uzawa, K. et al. Targeting phosphodiesterase 3B enhances cisplatin sensitivity in human cancer cells. *Cancer Med.* **2**, 40–49 (2013).
72. Seiler, S. E. et al. Obesity and lipid stress inhibit carnitine acetyltransferase activity. *J. Lipid Res.* **55**, 635–644 (2014).
73. Lasheras-Otero, I. et al. The regulators of peroxisomal acyl-carnitine shuttle CROT and CRAT promote metastasis in melanoma. *J. Invest. Dermatol.* **143**, 305 (2023).
74. Wang, Y. et al. Acetyl-CoA carboxylases and diseases. *Front. Oncol.* **12**, 836058 (2022).
75. Hong, H.-J. et al. ACACB is a novel metabolism-related biomarker in the prediction of response to cetuximab therapy inmetastatic colorectal cancer. *Acta Biochim. Biophys. Sin. (Shanghai)* **54**, 1671–1683 (2022).
76. Corbet, C. et al. Acidosis drives the reprogramming of fatty acid metabolism in cancer cells through changes in mitochondrial and histone acetylation. *Cell Metab.* **24**, 311–323 (2016).
77. Ding, R. et al. Utilising bioinformatics and systems biology methods to uncover the impact of dermatomyositis on interstitial lung disease. *Clin. Exp. Rheumatol.* **43**, 282–289 (2025).
78. Chen, C. et al. Pathogenic gene connections in type 2 diabetes and non-alcoholic fatty liver disease: A bioinformatics analysis and mouse model investigations experiments. *Nutr. Diabetes* **14**, 60 (2024).
79. Chen, J. et al. FTO-induced APOE promotes the malignant progression of pancreatic neuroendocrine neoplasms through FASN-mediated lipid metabolism. *Int. J. Biol. Sci.* **21**, 1478–1496 (2025).
80. Cenigaonandia-Campillo, A. et al. Vitamin-C-dependent downregulation of the citrate metabolism pathway potentiates pancreatic ductal adenocarcinoma growth arrest. *Mol. Oncol.* **18**, 2212–2233 (2024).
81. Che, L. et al. Valine metabolite, 3-hydroxyisobutyrate, promotes lipid metabolism and cell proliferation in porcine mammary gland epithelial cells. *Front. Nutr.* **11**, 1524738 (2024).
82. Guo, F. et al. M2-type tumor-associated macrophages upregulated PD-L1 expression in cervical cancer via the PI3K/AKT pathway. *Eur. J. Med. Res.* **29**, 357 (2024).
83. Vousden, K. H. & Lane, D. P. p53 in health and disease. *Nat. Rev. Mol. Cell Biol.* **8**, 275–283 (2007).
84. Bailey, P. et al. Genomic analyses identify molecular subtypes of pancreatic cancer. *Nature* **531**, 47–52 (2016).
85. Zhao, Y. et al. TP53 in MDS and AML: Biological and clinical advances. *Cancer Lett.* **588**, 216767 (2024).
86. Liu, J. et al. Lipogenic enzyme FASN promotes mutant p53 accumulation and gain-of-function through palmitoylation. *Nat. Commun.* **16**, 1762 (2025).
87. Yang, J. et al. PVRL2 suppresses antitumor immunity through PVRIG- and TIGIT-independent pathways. *Cancer Immunol. Res.* **12**, 575–591 (2024).
88. Li, A. et al. Single-cell RNA sequencing highlights the role of PVR/PVRL2 in the immunosuppressive tumour microenvironment in hepatocellular carcinoma. *Front. Immunol.* **14**, 1164448 (2023).
89. Maïza, H. et al. A novel 80-kD cell surface structure identifies human circulating lymphocytes with natural killer activity. *J. Exp. Med.* **178**, 1121–1126 (1993).
90. Sun, H. et al. Reduced CD160 expression contributes to impaired NK-cell function and poor clinical outcomes in patients with HCC. *Cancer Res.* **78**, 6581–6593 (2018).
91. Ni, L. & Dong, C. New B7 family checkpoints in human cancers. *Mol. Cancer Ther.* **16**, 1203–1211 (2017).
92. Liu, S. et al. The role of CD276 in cancers. *Front. Oncol.* **11**, 654684 (2021).
93. Deng, T. et al. Rapidly-manufactured CD276 CAR-T cells exhibit enhanced persistence and efficacy in pancreatic cancer. *J. Transl. Med.* **22**, 633 (2024).
94. Inamura, K. et al. Tumor B7–H3 (CD276) expression and survival in pancreatic cancer. *J. Clin. Med.* **7**, 172 (2018).
95. Chow, M. T. & Luster, A. D. Chemokines in cancer. *Cancer Immunol. Res.* **2**, 1125–1131 (2014).
96. Kadomoto, S., Izumi, K. & Mizokami, A. The CCL20-CCR6 axis in cancer progression. *Int. J. Mol. Sci.* **21**, 5186 (2020).
97. Liu, B. et al. Tumor-associated macrophage-derived CCL20 enhances the growth and metastasis of pancreatic cancer. *Acta Biochim. Biophys. Sin. (Shanghai)* **48**, 1067–1074 (2016).
98. Li, N. et al. C-C motif chemokine ligand 14 inhibited colon cancer cell proliferation and invasion through suppressing M2 polarization of tumor-associated macrophages. *Histol. Histopathol.* **36**, 743–752 (2021).
99. Kim, H. Y. et al. Uremic toxin indoxyl sulfate induces trained immunity via the AhR-dependent arachidonic acid pathway in end-stage renal disease (ESRD). *Elife* **12**, RP87316 (2024).
100. Kito, Y. et al. Potential of anti-leukotriene drugs as new therapeutic agents for inhibiting cholangiocarcinoma progression. *Molecules* **29**, 3379 (2024).
101. Alarcón-Sánchez, B. R. et al. A model of alcoholic liver disease based on different hepatotoxics leading to liver cancer. *Biochem. Pharmacol.* **228**, 116209 (2024).
102. Mohd Abas, M. D. et al. Advancements of gene therapy in cancer treatment: A comprehensive review. *Pathol. Res. Pract.* **261**, 155509 (2024).
103. Lord, C. J. & Ashworth, A. PARP inhibitors: Synthetic lethality in the clinic. *Science* **355**, 1152–1158 (2017).
104. Erratum: Overall Survival Results From the POLO Trial: A Phase III Study of Active Maintenance Olaparib Versus Placebo for Germline BRCA-Mutated Metastatic Pancreatic Cancer. *J Clin Oncol* **42**, 2112 (2024).
105. Kaufman, B. et al. Olaparib monotherapy in patients with advanced cancer and a germline BRCA1/2 mutation. *J. Clin. Oncol.* **33**, 244–250 (2015).
106. Burris, H. A. 3rd. et al. Improvements in survival and clinical benefit with gemcitabine as first-line therapy for patients with advanced pancreas cancer: A randomized trial. *J. Clin. Oncol.* **41**, 5482–5492 (2023).
107. Zhang, J. et al. BRCA1 orchestrates the response to BI-2536 and its combination with alisertib in MYC-driven small cell lung cancer. *Cell Death Dis.* **15**, 551 (2024).
108. Strebhardt, K. & Ullrich, A. Targeting polo-like kinase 1 for cancer therapy. *Nat. Rev. Cancer* **6**, 321–330 (2006).

Author contributions

YP conceived and designed the studies. LW, FL conducted the experiments. LW, FL,CC and YZ obtained and assessed the data. The first draft was written by FL. YP, FL, CC, and HH worked on editing and reviewing the manuscript. LW and YZ revised the manuscript. The study was supervised by YP. All authors have read and approved the article.

Funding

This study was funded by the Joint Funds of Scientific and Technological Innovation Program of Fujian Province (2020Y9081) and the National Natural Science Foundation of China (No. 82103310).

Declarations

Competing interests

The authors declare no competing interests.

Ethics approval and consent to participate

The study had obtained the approval of the Ethics Review Committee of Fujian Medical University Union Hospital (approval number: 2023KJCXC028). All participants were recruited from the Department of General Surgery of Fujian Medical University Union Hospital. Before enrollment, each participant was provided with detailed information about the study's objectives, procedures, potential risks, and benefits. Written informed consent had been obtained from all participants before any samples were collected. Participants were informed that they had the right to withdraw from the study at any time without any consequences to their medical care. Meanwhile, all tissue samples collected for this study had been de—identified to ensure patient confidentiality. The samples were labeled with unique codes, and all personal identifiers had been removed to protect participant privacy. The handling, storage, and analysis of the samples were carried out in accordance with the ethical guidelines and regulations set by the Ethics Review Committee. The study was conducted in compliance with the Declaration of Helsinki, and all procedures were monitored and approved by the Ethics Review Committee to ensure compliance with ethical standards.

Additional information

Supplementary Information The online version contains supplementary material available at https://doi.org/10.1038/s41598-025-99144-z.

Correspondence and requests for materials should be addressed to Y.P.

Reprints and permissions information is available at www.nature.com/reprints.

Publisher's note Springer Nature remains neutral with regard to jurisdictional claims in published maps and institutional affiliations.